

POLITECNICO DI TORINO



Master degree in Mechanical Engineering

Numerical Analysis of Internal Cooling Configurations for High-Pressure turbine Blades

Relatore

Prof.ssa Daniela Anna Misul

Prof. Mirko Baratta

Tutor aziendale

Ing. Marco Toppino

Candidato

Giorgio Mollo

Matr. 261386

Academic Year 2020/2021

Abstract

Gas turbines represent nowadays one of the most important sources of energy, covering a big slice of the energy need finding a good compromise between energy production and efficiency. Generally, as the system is conceived, to find the aforesaid compromise high temperatures needs to be reached. Thus, cooling mechanisms are adopted by spilling a percentage of the compressor mass-flow rate to refrigerate the areas mostly subjected to this high thermal stresses. Therefore, cooling phenomena represent one of the main subjects to be studied and elaborate in-depth avoiding or at least containing thermo-mechanical stress leading to fatigue cracks. The present thesis aims at investigating and increasing cooling effectiveness within an industrial gas turbine high-pressure blade by means of turbulators. The analysis took advantage of various articles about experimental procedure carried on in channels with this geometry variation, leading to heat transfer enhancement. It is worth saying that pressure losses are added to the system which in turn needs to be faced by increasing the pumping power and so to an efficiency reduction in its global meaning. Firstly, a Matlab® model has been developed implementing correlation trying to find an optimal configuration in terms of heat transfer enhancement and mass-flow rate reduction with respect to a geometry without ribs. Three different rib-turbulators configurations have been tested, each of them with the relative experimental correlation. The work continued performing a model validation by means of Computational Fluid Dynamics thanks to the StarCCM+ solver. Finally, the geometries which resulted to be validated were compared in terms of fluid-dynamic and thermal performances.

Sommario

Chapter 1	6
1. Introduction	6
1.1 Energy context.....	6
1.2 Joule-Brayton cycle and Efficiency considerations	7
Chapter 2	11
2. Gas-turbine blade cooling	11
2.1 Importance of cooling	11
2.2 Internal cooling	13
2.2.1 Rib-roughened channels.....	13
2.2.1 Impingement cooling.....	15
2.2.3 Matrix cooling	16
2.3 External cooling	17
2.3.1 Film cooling	18
2.4 EthosEnergy Group TG20B7/8 Turbine	19
Chapter 3	20
3. Introduction to model validation	20
3.1 State of art: Literature review.....	20
3.2 Correlation validation with optimal evaluation.....	21
3.2.1 Rectangular ribs configuration	21
3.2.3 Semicircular ribs configuration.....	27
3.3 Final considerations.....	31
Chapter 4	34
4. Star-CCM+ and mathematical model.....	34
4.1 Governing equations	34
4.1.1 Continuity equation.....	34
4.1.2 Momentum equation	34

4.1.3 Energy equation	35
4.2 Turbulence modelling	35
4.2.1 RANS equations.....	35
4.3 Preprocessing	39
4.3.1 Rectangular ribs problem – 3D Geometry	39
4.3.2 Semicircular ribs problem – 3D Geometry	41
4.3.3 Meshing.....	41
4.3.4 Continua and regions	44
4.4 Postprocessing.....	47
4.5 Results comparison	48
4.5.1 Turbulence discussion.....	51
4.5.2 Mesh refinement	51
5. Models Validation.....	53
5.1 Domain reduction: 2D.....	53
5.1.1 Surface division.....	55
5.2 Structured Mesh	56
5.3 Validation.....	59
5.3.1 Physics settings and boundary conditions.....	60
5.4 Results discussion – Rectangular ribs configuration	62
5.5 Results discussion – Semicircular ribs configuration	67
Chapter 6.....	72
6. Final comparison and Conclusions	72
6.1 New mesh.....	73
6.1.2 Physics and Boundary conditions	74
6.2 Results in terms of Nusselt number	75
7 Conclusions.....	77
7.1 Summarizing conclusions	77

7.2 Future studies	77
References	78

Chapter 1

1. Introduction

1.1 Energy context

The first industrial revolution represented a turning point for the whole world, since mass energy production had been possible thanks to the development of new technologies, which firstly took advantage of combustion with steam engines adopting fossil fuels. To that event could be assigned the credit of a completely new way to live this world.

The following years were marked by a race for the creation of even bigger and faster machines, which allowed to have a high level of benefits and in a way left the population out from a primitive way of living. Thus, the clear increase in energetic need is one of the main problems of the last century, considering the demographic, industrial and economic growth of the whole world.

How to deal to this problem represented the real challenge to be faced in the twentieth century for engineers and scientists all over the world.

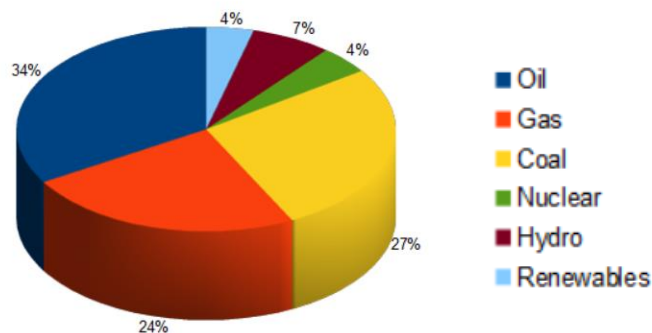


Figure 1.1 – Global energy consumption in 2018

As it can be noticed from the cake chart, a great amount of energy is still nowadays supplied by fossil fuels.

Combustion mechanisms are adopted in order to take advantage of this primary source of energy, as a chemical reaction it implies combustion products classified as pollutant, which in turn have an impact on the environment so as on the human life on earth.

During the last decades the development of renewable energy played a fundamental role not only for what regards the total absence of pollutant agents during the energy generation but also because opened the door to a totally new field of study, just to mention one they started to take advantage of the most important energy source which permits life on earth, the sun.

Even if they allow to produce clean energy, their use has been confined to a low production percentage with respect the entire energy need in many countries, due to their low efficiency and high plant costs.

Therefore, since the need of energy increases year by year, many solutions have been developed and gas turbine represents probably one of the most important.

In this context, the object of the present thesis is the electrical power generation by means of turbo-gas plants, which can guarantee:

- high output power
- increasing efficiency
- low pollutant emissions

Since the working mechanisms and plants have been introduced, lots of studies carried out ways to further increase efficiency and power output leading to a series of scenarios which act differently on the component of the plant itself with the same result.

One can think to mention the increase of the turbine inlet temperature as the main method to increase in output as well as the increase in compression ratio, the latter results having more structural limitations.

It is worth to say that the research and development of turbo-gas plants led to innovations in other fields, for instance the need of more resistant materials.

1.2 Joule-Brayton cycle and Efficiency considerations

As mentioned before, turbo-gas plants represent the most reliable and efficient way to produce electrical power. The working fluid is air and the thermodynamic cycle exploited is the Joule-Brayton: open cycle with a single shaft machine.

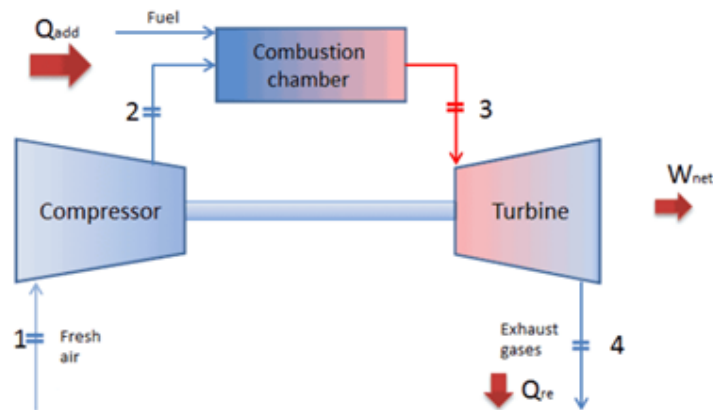


Figure 1.2 - Turbo-gas plant in open circuit

It is made-up by four components:

- compressor, needed to increase pressure of air
- burner, in which combustion takes place
- turbine works with high temperature and pressure fluid, connecting the compressor and the generator on a shaft
- generator, provides to the conversion of rotational movement in electric power

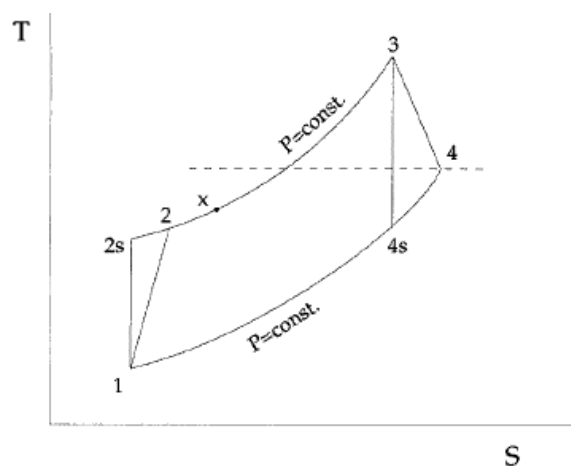


Figure 1.3 – Real and ideal Joule-Brayton cycle on a T-s diagram

In the plot above are depicted both the real and ideal Joule cycles, the first represented by states 1-2-3-4 in sequence, the latter by 1-2s-3-4s where it follows the isentropy line in compressor and turbine transformations either.

Air is sucked in by the compressor (1) which provides the increase in pressure from inlet to outlet (2), then the combustion chamber receives the highly-pressurized air. The mainstream flow is now

a mix of air and fuel, the burner provides combustion increasing a lot temperatures, reaching the maximum temperature in the cycle (3). Once the combustion occurs the flow shows high pressure and temperatures, respecting the requirements of the turbine to work, so the expansion starts thus producing a power output; finally the burned gas are exhausted in air (4).

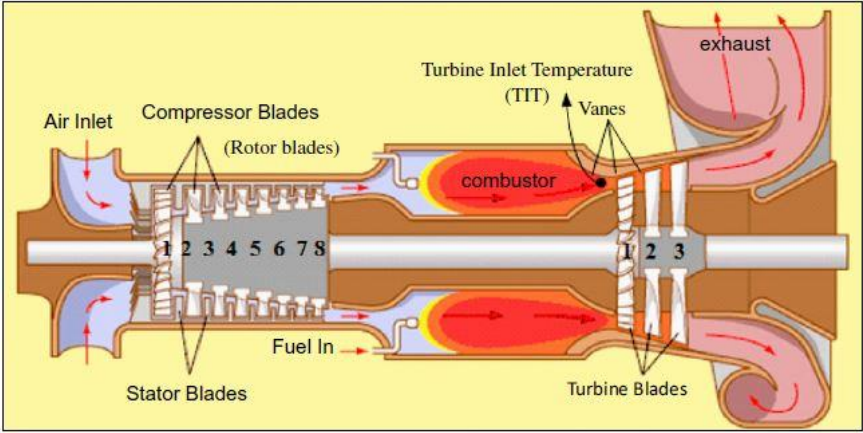


Figure 1.4 - Cutaway view of an industrial gas turbine engine

The parameters of crucial importance need to be specified, they are basically the compression ratio and the turbine inlet temperature (TIT). As a matter of fact, they influence performances of the machine in its whole; to mention a few, obtainable power output and stage efficiency, the latter directly connected to the global one.

An efficiency augmentation is then possibly reached by increasing either the compression ratio or the turbine inlet temperature. From the following picture it is clear how the maximum temperature influences the global efficiency and so the power production itself.

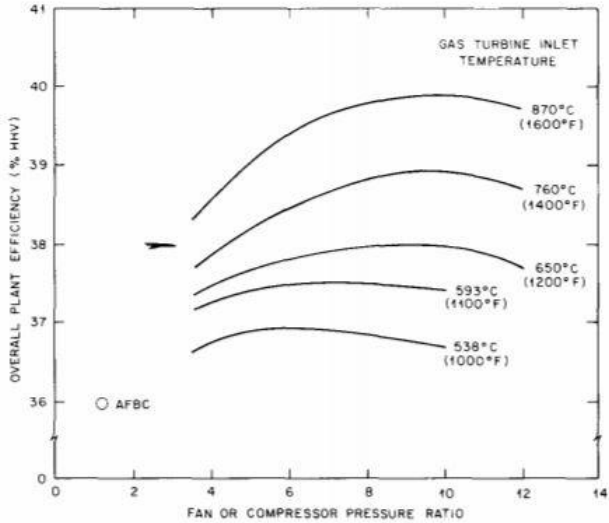


Figure 1.5 - Overall efficiency function of compressor pressure ratio with varying TIT

Whatever is chosen, of course it implies dealing with occurring problems within the machine. In case of growth in compressor ratio would lead to a serious increase in stresses which may exceed the limit of sustainability of the materials, while in case of rising TIT strong thermo-mechanical stresses are to be faced.

In both cases, the structure functioning is seriously compromised together with its designed-life service.

To solve this problem an investigation on high performance materials with the purpose of containing stresses was conducted, ensuring high thermo-mechanical resistance while keeping almost unaltered the mechanical properties with an increasing temperature. Unfortunately, that did not represent a good solution, leading to a reduction in global efficiency and without a good degree of reliability.

Then, internal blade cooling for both stator and rotor has been introduced guaranteeing a high-life service of the component. This technique, since its introduction in the early 50s, allowed to increase the plant efficiency by working with high turbine inlet temperatures and guaranteeing at the same time very high reliability and an acceptable working life of the component.

Chapter 2

2. Gas-turbine blade cooling

2.1 Importance of cooling

The *blade cooling* was conceived to keep metal temperature of turbine blades under a critical limit, property of the material itself, usually done at the first turbine stage (see Figure [1.4]) which results to be in the worse conditions in terms of thermal stresses being directly connected to the high temperatures of the burner outlet.

This can be done by spilling a certain percentage of mass flow rate from the first compressor stages, where the fluid is at low temperature, then carrying it to the first turbine stage and further divided to the other stages thanks to a series of channels. It is important to note that this extraction can reduce the thermal efficiency and power output of the turbine engine.

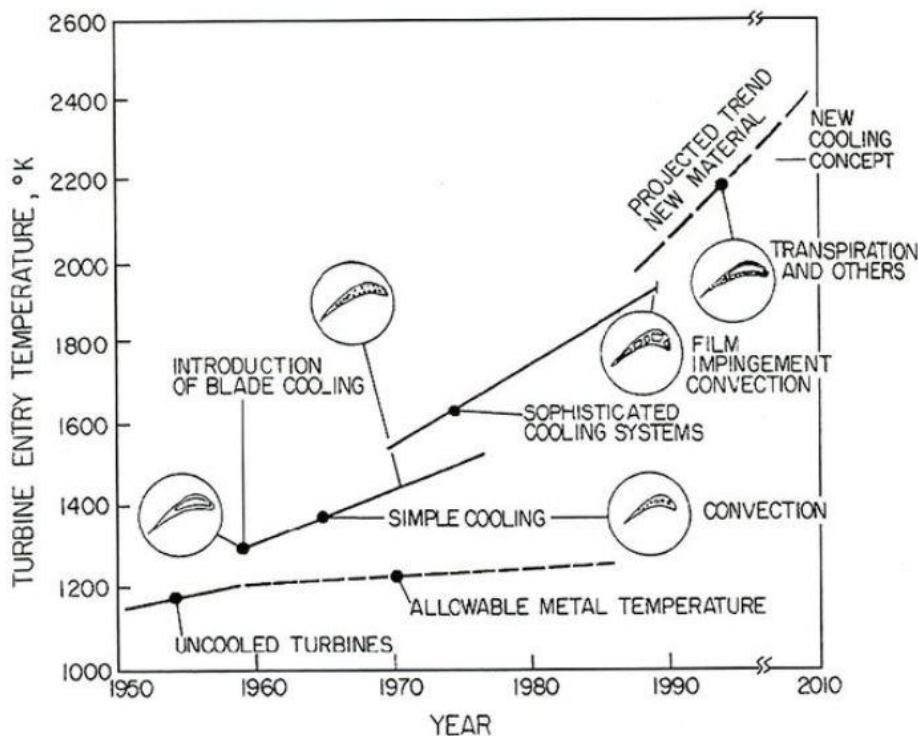


Figure 2.1 - Variation of turbine entry temperature over recent years [2]

From Figure [2.1] it is clear that with the introduction of cooling techniques the temperature reached in the burner has been increased starting from the 1100 K of the early 50s and reaching

then in the 70s temperatures equal to 1700 K; finally with very fine cooling techniques the most advanced gas turbine plants allow to touch till 2000 K nowadays.

From the point of view of the heat exchange, convection occurs between the fluid and the metal while through conduction the heat is transferred in the whole blade.

Today various techniques of cooling exist aim at containing the turbine inlet temperature, they all share the same goal but with different applications are used and controlled in order to adapt themselves to the particular machine or zones where they are applied to. In the following image are depicted the cooling techniques used for different parts of the blade.

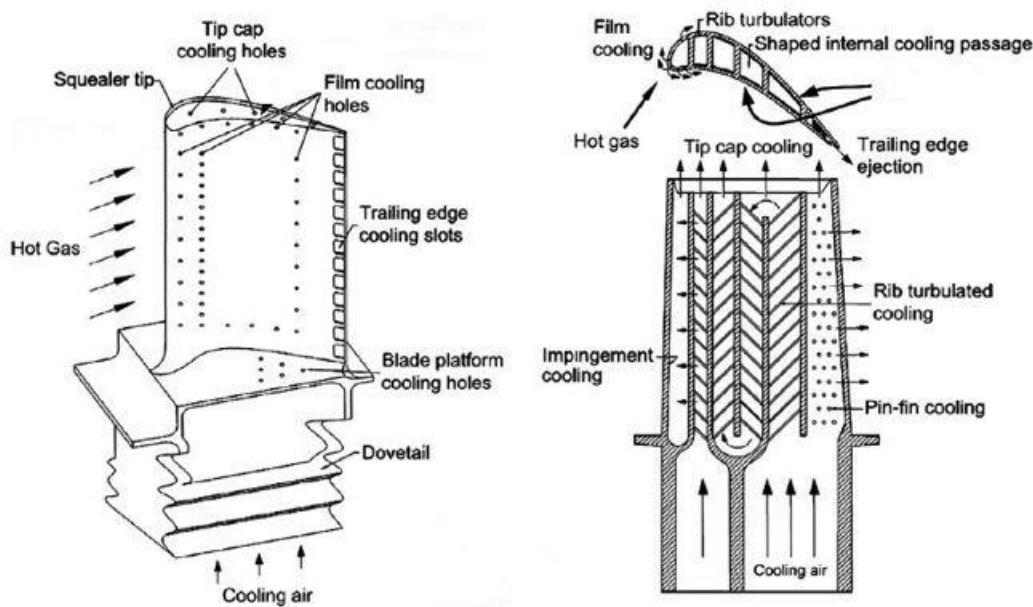


Figure 2.2 - Cooling techniques for leading edge and blade tip (sx) and for suction and pressure sides (dx), from “Evolutionary numerical simulation approach for design optimization of gas turbine blade cooling channels”, N.R. Nagaiah and C.D. Geiger, 2013

Two big categories are recognized, namely:

- Internal cooling
- External cooling

As it is easily to understand, they differ depending on how the refrigerant acts on the surfaces to be cooled down. If the contact with the fluid occurs at the external surface of the object (e.g. a turbine blade) it is about *external cooling*; when, on the other hand, cavities are obtained in the component body it is the case of an *internal cooling*.

It is worth to underline that one technique does not exclude the other one. As a matter of fact, they can be combined resulting in a really big cooling action on the surfaces. This solution of course does not correspond to a usually adopted configuration because they are prescribed to cases which works in harsh conditions, for instance aerospace ones, requiring high costs due to the great accuracy needed.

2.2 Internal cooling

The study concerning cooling techniques for industrial gas turbine surely found its basis on the internal cooling. As previous mentioned they consist in a series of channels obtained inside the blade which extend from the root to the tip of the blade itself. So, the pressurized refrigerant flows within these cavities taking advantage of convection phenomena between the fluid and the blade internal wall, with the goal of reducing uniformly the entire body temperature and keeping it under critic values in order to avoid unsustainable thermal stresses.

The heat exchange occurring thanks to convection could be easily managed, since convection, as it stands, owes its ability to remove heat on the surface geometry it is passing through and on the kind of motions that are triggered.

It is quite obvious to understand that geometry plays a leading role in this field, acting to increase the heat transfer. As a matter of fact, surface variation will be considered from now on as the main feature for the internal cooling.

Particularly it is appropriate to remind that a direct connection holds between the fluid velocity and the convection heat transfer coefficient. Having said that, it is of generally understanding that the fluid velocity influences most of all the motions within the channel. Turbulence is often required for such a cooling technique, enhancing the convection phenomena by acting on augmentations for the convective heat transfer coefficient and so on the heat exchange.

Therefore, the velocity field combined with the geometry, can be manipulate to achieve the desired results.

2.2.1 Rib-roughened channels

This technique takes advantage of the sudden change in geometry, which would generate the turbulence and so an enhancement in the heat transfer within the channel. This configuration of

channels surfaces represents an obstacle for the fluid flow, it aims at generating turbulence but even to keep it for the whole fluid path. The stream experiences a strong deviation imposed by the obstacle, forcing it to adapt to the decreased channel cross section. It is accelerated to pass the rib which implies a downstream expansion.

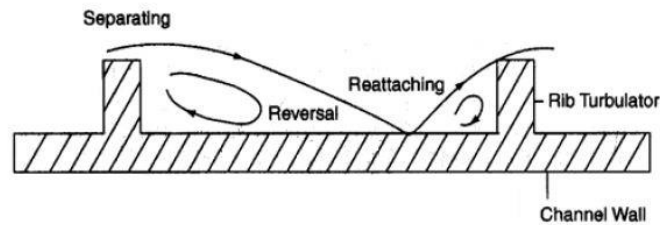


Figure 2.3 - 2D scheme of a ribbed channel with rectangular ribs

Both separation at the rib top and reattachment to the flow between the ribs, disturb the boundary layer increasing turbulence thus leading to an increase in heat transfer. The cooling occurs when there is a mixing action between the fluid elements at the boundary with the cooler in the middle of the channel. As it stands, from the operational point of view, the turbulence control is guaranteed by acting on the various geometric parameters which define the rib as an obstacle, they are: the pitch (between one rib and the next in the flow direction), the rib height, the roughness (usually defined as the ratio between the rib height and hydraulic diameter).

Of course, using ribs to enhance heat transfer capability implies pressure drop; this brings to another important step: get a good compromise between increasing heat transfer and contain losses in a certain range. Again, the rib-roughened internal cooling passages cause turbulence in the coolant as the coolant passes over and around the ribs (or turbulators). The turbulent air removes a fraction of the heat conducted in suction and pressure sides from the blade.

The increase in heat transfer coefficient is directly proportional with the increase of the Nusselt number, which represents the actual parameter to be maximized.

Rib roughened channels are mostly adopted for suction and pressure sides of the blade, so they are used to act basically in the whole length; this method is often combined with others mainly devoted to the cooling of leading and trailing edges, as will be clear later.

2.2.1 Impingement cooling

Conceptually speaking, it works the same as the rib-roughened channel, the main difference stands on how the fluid flow is conveyed within the channel. The stream is forced to pass through a series of holes (forming the so called jet plate), they are useful to enhance the pressure of the fluid flow and so have an higher impact on the boundary layer formed on the target surface resulting in a faster cooling action with a sudden reduction in temperature. Impingement cooling as it is conceived, is able to reach higher heat transfer coefficient with respect to rib-roughened channels.

This technique is used for its characteristics mostly for cooling of the leading and trailing edges, where the temperature is higher and hold more limitations about pressure drop, thus a gain in temperature reduction seems to be more difficult.

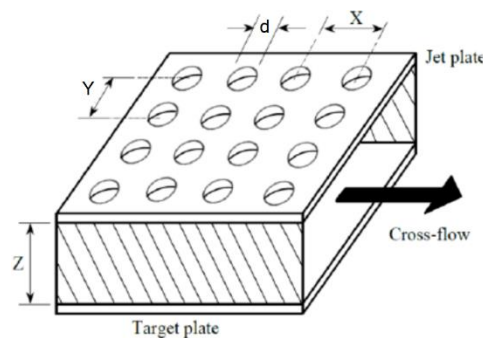


Figure 2.4 - Qualitative scheme of an impingement cooling system

This increase in heat transfer coefficient is due to the turbulent nature of the jet impinging the surface and the thickness of the boundary layer. The cooled surface is called target plate. Various parameters can be modified in order to control the system, namely: number of jets (holes in the jet plate), jet hole configuration and jet angle of attack.

The impingement geometry is mainly described by the hole diameter and the distance between jet orifice and target plate. The flow is divided into three regions: free jet region, stagnation region and wall jet region. And in turn the *free jet* can be subdivided in other three zones: potential core, developing and fully developed.

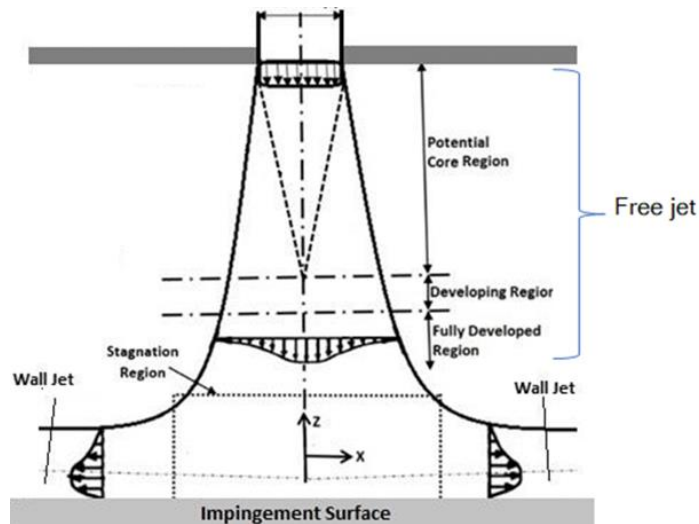


Figure 2.5 - Flow evolution during impingement

- The *free jet region* is the one characterized by the nozzle configuration and develops following the input parameters. Potential core basically follows the flow trend from the nozzle without being affected by the surrounding air, while the developing and fully developed zones are generated from the mixing with air and generate turbulence.
- The *stagnation region* is generated from the impact of the jet with the target plate. Theoretically, it should not allow any heat transfer but in reality it is not so steady and the stagnation point keeps moving: in this region the heat transfer reaches a maximum value.
- In the *wall jet region* the flow is parallel to the plate and the thickness increases due to the generation of a boundary layer. It could be reached a second heat transfer maxima for certain Reynolds numbers.

Among all the techniques which take advantage of convection heat transfer, the latter results to get the best efficiency in terms of cooling power.

2.2.3 Matrix cooling

The last internal cooling method that will be described is the matrix cooling. It is composed by two opposite layers of angled ribs. The effect on turbulence is quite the same of a rib-roughened channel but actually the system happens to be more complex due to the fact that the flow continuously changes in direction following the ribs configuration, as it is clearly described from Figure [2.6].

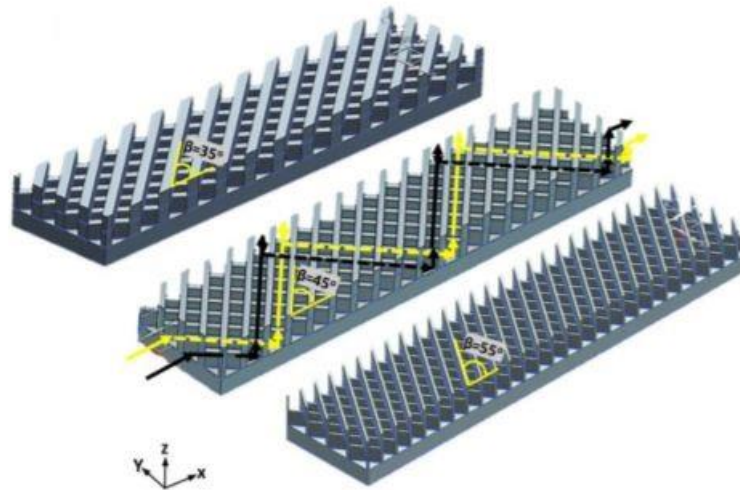


Figure 2.6 Matrix cooling scheme

The turbulence here is triggered when the flow passes from one channel to another by swirling. The heat transfer is increased thanks to combined effect of inlet, where a new boundary layer is developed, together with the higher surface area of longitudinal ribs. A new parameter is now considered such as the angle β formed by ribs with respect to the flow direction, which has an influence on the heat exchanges as well.

Two configurations can be distinguished, namely: open matrix and closed matrix. The first one allows various streams coming from different channels to mix, while the latter does not expect the different flows to encounter each other. In open matrices the flow is axial, while in closed it is radial. This technique is often used for trailing edges.

2.3 External cooling

With the development of technology and the following increase of power in machines, it has been of fundamental importance developing other strategies to face the problem regarding temperatures. The internal cooling which provided such great benefits was not enough anymore to keep temperatures in blades under a critical value, so the need of end up with other forms of cooling methods represented a big challenge to engineers in the field. As previously introduced, external cooling ensures reductions in temperature which are a lot higher with respect to that gained with the internal one. Since the end of 70s and mostly during 80s, external cooling of blades and vanes, has reached great aims. It implied at the same time high costs and aerodynamic losses since the refrigerant ends up mixing with the working fluid. The most important technique in this field is the *film cooling*.

2.3.1 Film cooling

This method found its application when blade temperatures are too high and there is the need to dump thermal stresses, often combined with such an internal cooling technique. It provides a thin layer of refrigerant on the blade to protect it from combustion products, keeping metal temperature under critic values. The bleeding air is extracted from holes obtained on the blade with the right pressure that can ensure the total coverage of the body. The extraction pressure needs to be evaluated with great accuracy, very slight changes could compromise the functioning of this method. As a matter of fact, it could happen that the refrigerant comes to mix with the flue gas without exercise any kind of protection for the blade. In the following picture there is an overview of the film cooling functioning.

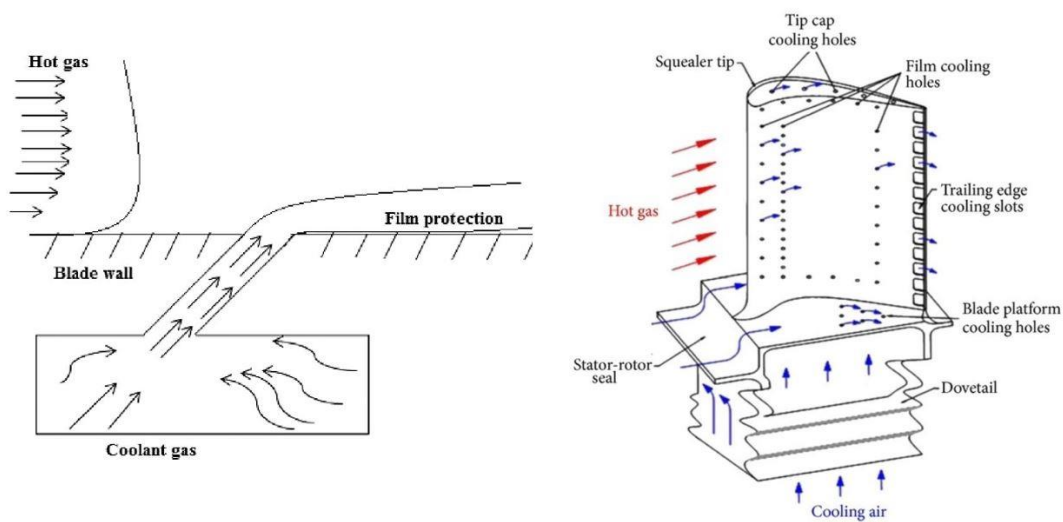


Figure 2.7 - Film cooling generation (sx) and its application on a blade (dx)

From Figure [2.7, dx] at the right, it is possible to see that the bleeding holes are repeated along the whole blade profile, this is useful to ensure that the film cooling generated will not die out easily. This continuative action of cooling can guarantee the performance mentioned before about the high regenerative power of this technique. Again, are clearly defined the path followed by the hot gas and the cooling air. Having said that, a good design of the system should be done in order to avoid any issue related to the discontinuity of cooling.

2.4 EthosEnergy Group TG20B7/8 Turbine

TG20B7/8 is a gas turbine whose rated power is 48 MW, produced by EthosEnergy Group and derived from Westinghouse project. The machine is characterized by 19 compression stages; a pressure ratio of 15.4 is reached. Compressor set-up is the result of a recent redesign, carried out with commercial software for streamline flow analysis for turbomachinery. The turbine section, as typical of this machine size, is composed by 3 expansion stages. Turbine Inlet Temperature has been increased from 788 up to 1129° C. Problems were identified in the cooling vane insert, dust particles clogged the cooling vane insert and by having a reduced coolant mass flow after several cycles statoric and rotating blades went colliding. So, a solution needed to be found to avoid that kind of problem. The cooling air is extracted from combustor shell and sent directly to the first vane of the turbine, with this system the clogging formation is totally avoided arising the machine reliability.

Therefore, in row 1 vane cooling system, two inserts have been adopted containing multiple holes so impingement on leading edge region and film formation around the profile are exploited.

The efforts of the present work are finalized to find a better solution for the cooling operation in the turbine section.

Chapter 3

3. Introduction to model validation

3.1 State of art: Literature review

Since its introduction internal cooling, or most generally blade cooling, has been an interesting topic for all researchers working with gas turbines. The issues related to the developing cooling techniques were faced as a first attempt with experimental procedures in the past decades, only with the help of software specialized in flow analysis has been possible in recent years to have a correct evaluation of parameters and how they influence the heat exchange without reproducing the real environment with specimens in laboratory.

The present work will be focused only on internal cooling of gas turbine blade, particularly on rib-roughened channels trying to exploit the actual potential that previous studies have already predict. Specifically, going through the influence of this geometry variation within circular channels. This aspect plays a fundamental role due to the fact that a change in duct configuration implies a variation in the parameters that actually influence the thermodynamic characteristics of the flow.

Therefore, a literature review was crucial in order to have an idea of the state of art and to develop in such a way the basis of a possible future use of the tested models.

Many studies regarding rib-roughened circular channels are present in literature, most of them have been conducted with rectangular rib configuration, a small portion focused their attention on different kinds of rib surface as well as on the rib angle of attack (evaluated with respect to flow direction). All of them had as final purpose the development of correlations which could describe the fluid flow in that kind of channels. Following, a classification of them will be made. In order to do so, the main geometric and heat transfer parameters need to be clarified to have a good understanding of the matter. From a geometric point of view, the main parameters which influence the flow motion are rib-to-height ratio e/D and rib pitch-to-diameter ratio p/e . Later results will be discussed in terms of heat transfer, through Nusselt number, and friction factor.

Having said that, a first approach to the subject dates back to the early 60s when Webb, Eckert and Goldstein (1970) made experiments by varying the Reynolds number (in a range from 6.000 to 100.000) and looking on how heat transfer parameters changed. The main features of this technique are coherent among all the different studies; generally, increasing the rib-to-height ratio

results in heat transfer enhancement and at the same time corresponds to an increase in friction factor which can be related directly to a pressure losses increase. For what regards Reynolds number it happens the same, with increasing values heat transfer results to be higher.

This study built the basis of the future work even when looking to other geometries because in order to work out correlations it took advantage of previous studies about the generation of a boundary layer which develops near to the rib and wall. This aspect happens to be really important mostly when the fluid motion becomes turbulent due to vortex generation and a missing linearity governs the flow. Consequently, tests were performed by Gee and Webb (1980) with angled ribs obtaining almost the same values of heat transfer with respect to Webb et al. but with a significative reduction in friction factor. On the other hand, while developing first model correlations for rectangular ribs other geometries were tested. It is worth to mention the semicircular rib configuration tested by San and Huang (2006), evaluating parameters in a limited range of Reynolds number (4.608 to 12.936) and achieving high values of Nusselt combined to quite low friction losses.

3.2 Correlation validation with optimal evaluation

The correlations developed from experimental results have been taken as a reference to verify such results from a mathematical point of view. First of all, after having considered a lot of different studies were chosen three main configurations and then make comparisons among them, in terms of both heat transfer and friction, namely:

- Rectangular ribs configuration;
- Semicircular ribs configuration.

Experimental results and correlations respectively taken from Webb et al. [4] and San and Huang [5].

3.2.1 Rectangular ribs configuration

As said before, the article studying rectangular ribs influence on fluid flow characteristics has represented a basis for other studies in the field, so as for this thesis. A lot of parameters included in the equations were experimentally defined in order to simplify the description of what actually happens. For some parameters, due to this, does not exist a general equation for all the fluid's conditions and sometimes values should be read on experimental plots.

Thus, correlations were implemented on Matlab to end up with a graphical representation of results and then to make comparisons.

The equations derived from experiments are:

$$f = \frac{2}{\left[2,5 \cdot \ln\left(\frac{D}{2e}\right) + u_e^+ - 3,75\right]^2} \quad (3.1)$$

$$St = \frac{f/2}{1 + \sqrt{f/2} [\bar{g} \cdot Pr^{0,57} - u_e^+]} \quad (3.2)$$

$$Re = e^+ \frac{\sqrt{2/f}}{e/D} \quad (3.3)$$

$$Nu = Re \cdot St \cdot Pr \quad (3.4)$$

Where u_e^+ is the roughness Reynolds number evaluated as $\frac{e^+}{\left(\frac{p}{e}\right)^{-0,53}}$ used to account for friction data.

Then \bar{g} , used to account for heat transfer data evaluated as $4.5 * (e^+)^{0,28}$.

From the following image is clear that correlation overwrite quite good the values from experiments.

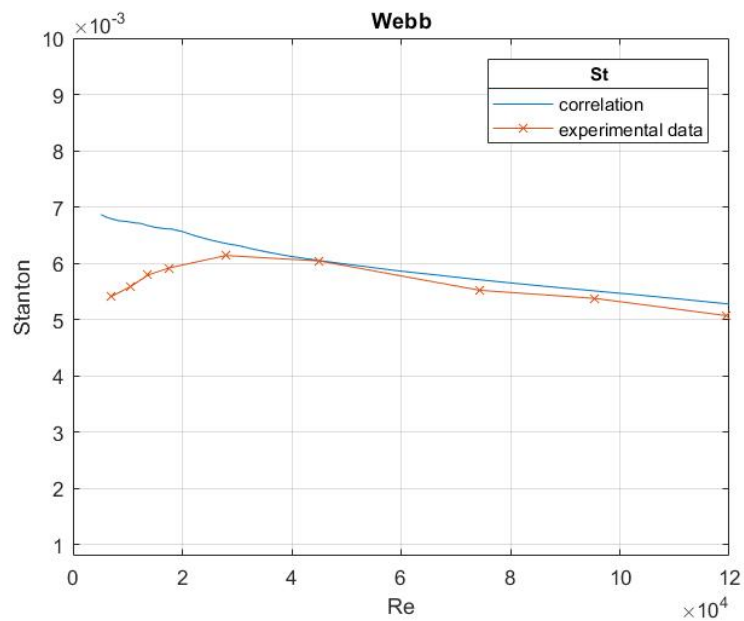


Figure 3.1 - Comparison between experimental results and correlation derived for rectangular configuration

Later, with the goal of expanding the work and give a suggestion for a possible development, correlations were carried ahead of the validation alone. The purpose was to find an optimal case for the rib geometry, maximizing the heat transfer coefficient and at the same time containing the friction factor. The previously mentioned geometric parameters will now come to help describing the results. Basically, have been chosen ranges for the ratios e/D and p/e , evaluating for each value which were the results in terms of Nusselt number and friction factor.

- $0,01 < \frac{e}{D} < 0,04$
- $10 < \frac{p}{e} < 40$

After having computed all the trends for each value of the two ratios, the best conditions are considered and are reported in following pictures.

Firstly, by keeping constant the ratio e/D by varying the rib-to-pitch ratio, has been found an optimal condition for which best results in terms of heat transfer are reached with quite good trends for friction as well. It corresponds to a geometry with rib height-to-diameter ratio equal to 0,01.

- Constant $e/D = 0,01$ with varying $p/e = 10 \div 40$

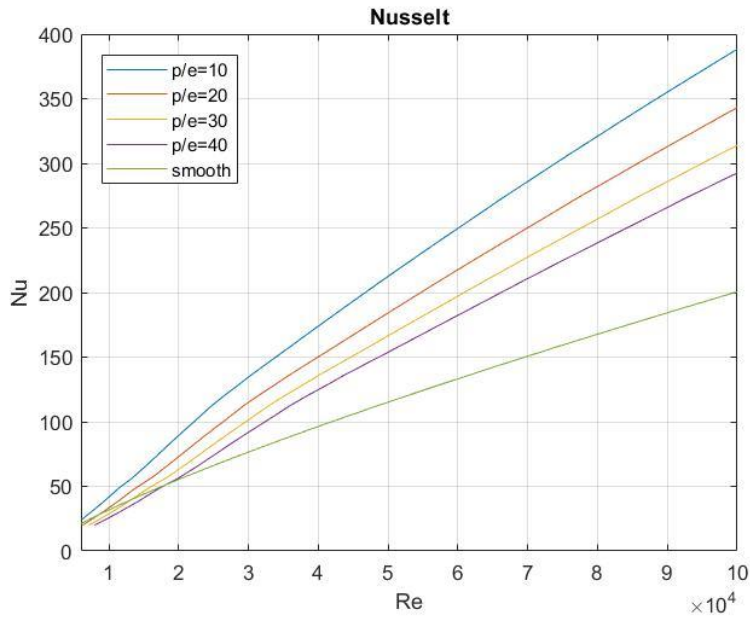


Figure 3.2 - Nusselt number for $e/D = 0,01$ and $p/e = 10 \div 40$

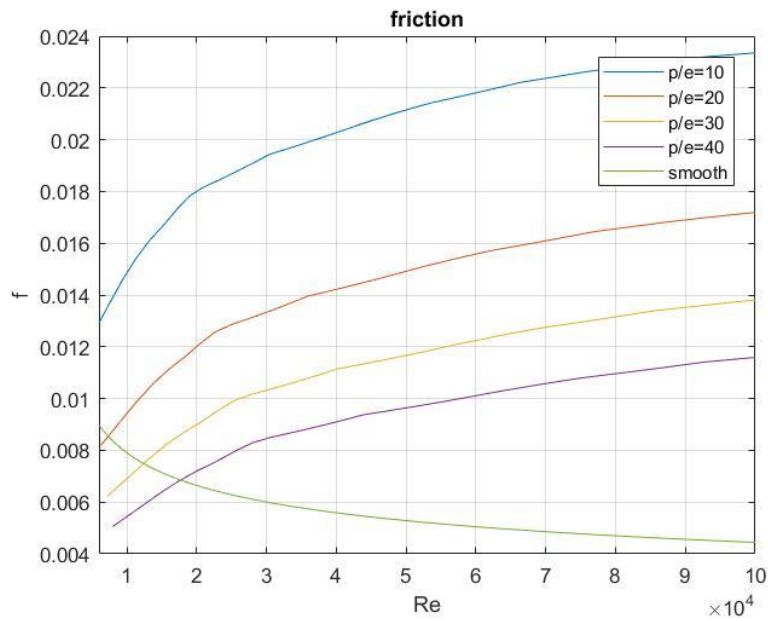


Figure 3.3 - Friction factor for $e/D = 0,01$ and $p/e = 10 \div 40$

Similar procedure is performed for rib pitch-to-height ratio, keeping it constant to a value in the range and let varying e/D . It is found that an optimal condition exists for $p/e = 10$.

- Constant $p/e = 10$ with varying $e/D = 0,01 \div 0,04$

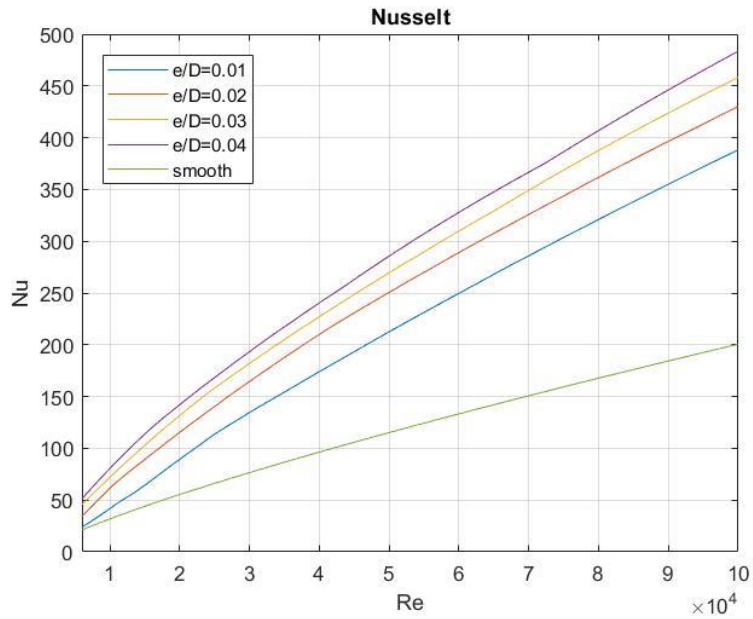


Figure 3.4 - Nusselt number for $p/e = 10$ and $e/D = 0,01 \div 0,04$

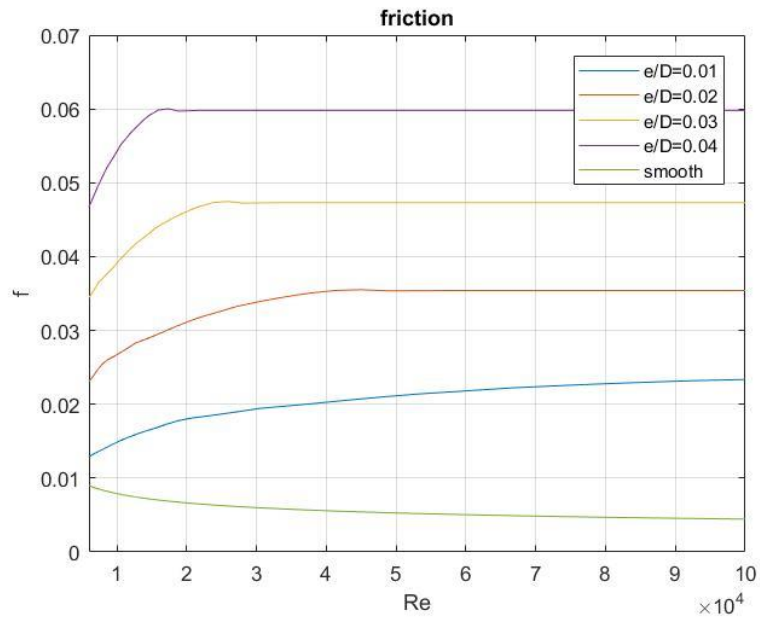


Figure 3.5 - Friction factor for $p/e = 10$ and $e/D = 0,01 \div 0,04$

All the curves are compared always with the *smooth case*, considering a channel without ribs. The values of the smooth friction factor f_s and smooth Nusselt number Nu_s are evaluated as:

$$f_s = \frac{0.079}{Re^{0.25}} \quad (3.5)$$

$$Nu_s = 0.023 \cdot Re^{0.8} \cdot Pr^{0.4} \quad (3.6)$$

Finally, by looking at the plots the *optimal configuration* is chosen where a real gain is obtained, in this case this is equal to:

- $\frac{e}{D} = 0.01$
- $\frac{p}{e} = 10$

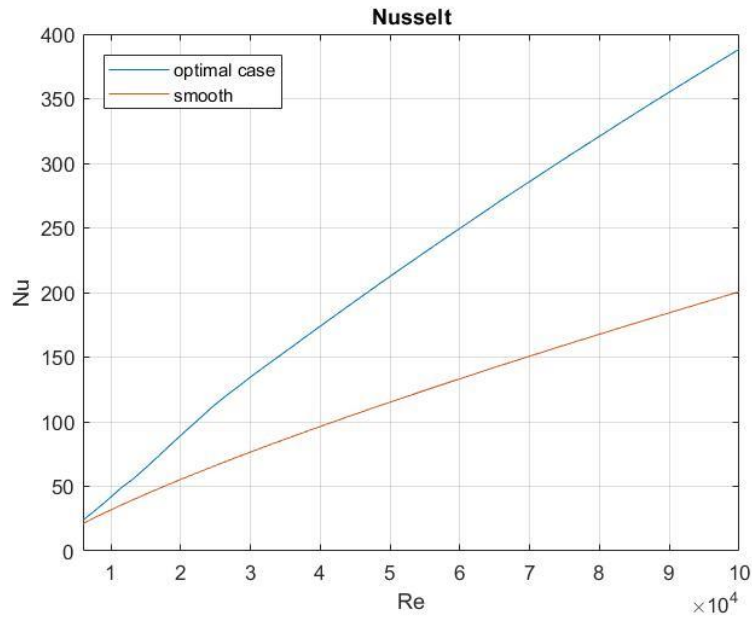


Figure 3.6 - Optimal configuration for rectangular ribs in terms of Nusselt number

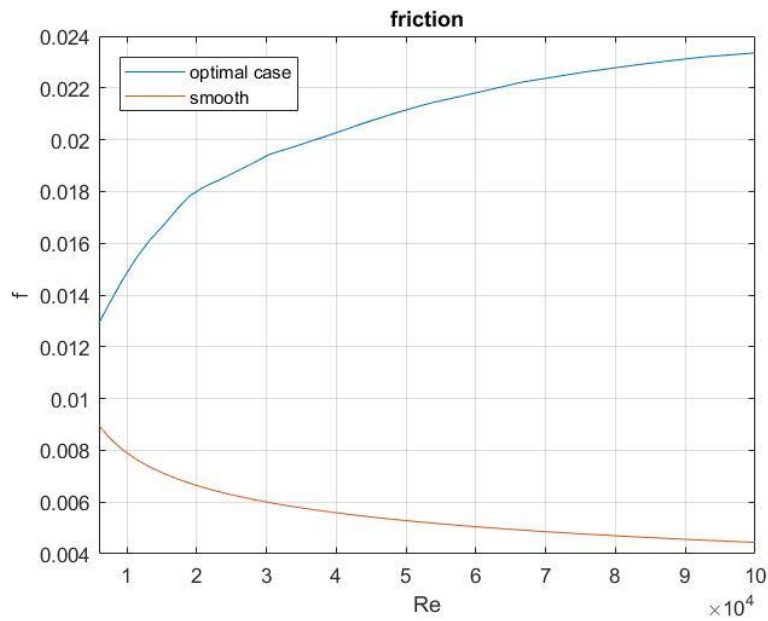


Figure 3.7 - Optimal configuration for rectangular ribs in terms of friction factor

3.2.3 Semicircular ribs configuration

This case is much different with respect to the previous two because there is a variation in the shape of the rib itself, it is no more rectangular but now looks semicircular, as in the following picture:

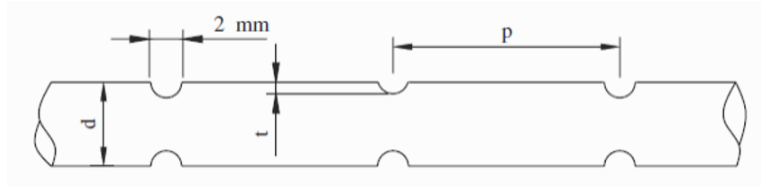


Figure 3.8 - Sketch of a ribbed channel with semicircular shaped ribs

Here, J.Y. San and W.C. Huang developed correlations from experimental data. They tested in a really small Reynolds number range (4608 ÷ 12936) their channels ending up with a set of equations accounting for friction and heat transfer, always in form of Nusselt number:

- For $0,015 \leq e/d \leq 0,05$

$$f = 0,0023(e/d)^{1,04} e^{-0,26(p/d)} (Re) e^{-1,44 \times 10^{-4} Re} \quad (3.7)$$

- For $0,057 \leq e/d \leq 0,143$

$$f = 0,132(e/d)^{2,55} e^{-0,26(p/d)} (Re) e^{-1,44 \times 10^{-4} Re} \quad (3.8)$$

And finally, for the evaluation of Nusselt:

$$Nu = 0,0072(Re)^{1,05} (p/d)^{-0,15} (e/d)^{0,333} \quad (3.9)$$

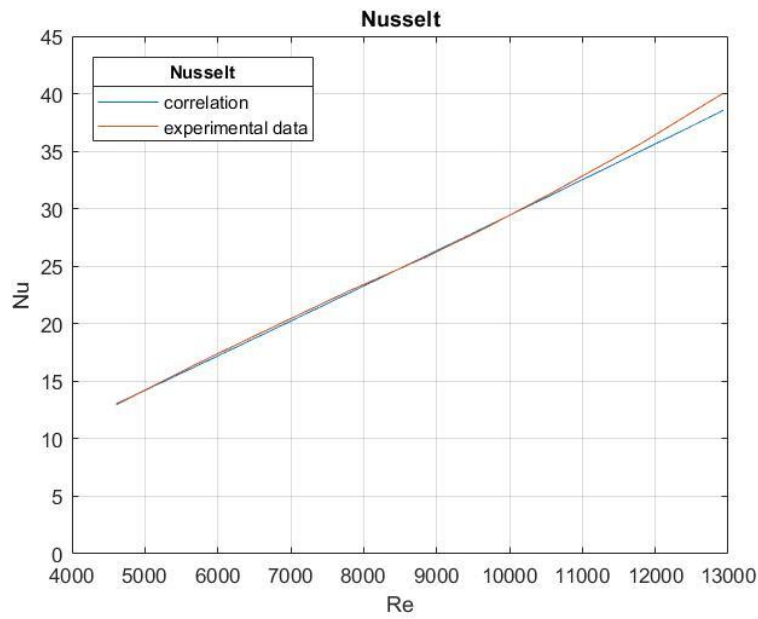


Figure 3.9 - Comparison between experimental results and correlation derived for semicircular configuration

Hence, an optimal configuration was the final goal with this configuration as well. As for the previous studies, has been kept constant in a first attempt the rib height and so the ratio e/D and then the rib pitch with p/e .

- Evaluating the effect of rib pitch keeping constant $e/D = 0,01$, with $p/e = 10 \div 40$

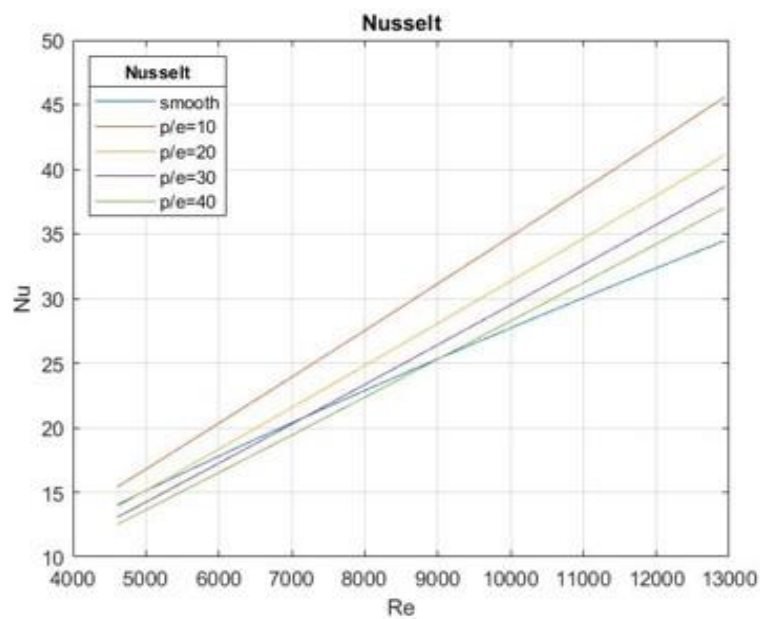


Figure 3.10 - Effect of rib pitch on Nusselt number

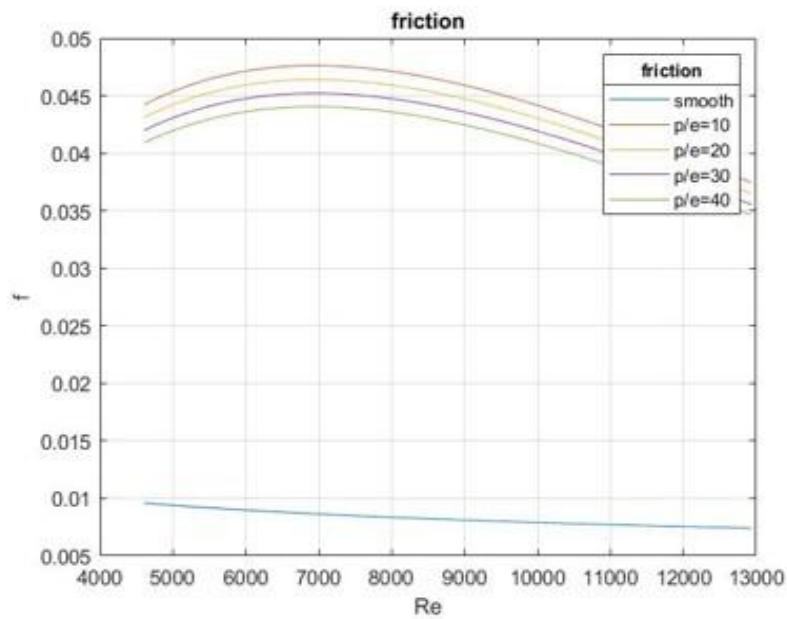


Figure 3.11 - Effect of rib pitch on friction factor

The rib pitch-to-height ratio chosen by comparing the curves is $p/e = 10$, because it shows a remarkable increase in Nusselt number. Regarding the friction factor it takes the highest values, it has been chosen because the actual percentage difference with respect to other values of the ratio is really small.

- Effect of rib height keeping constant $p/e = 10$, with $e/D = 0,01 \div 0,04$

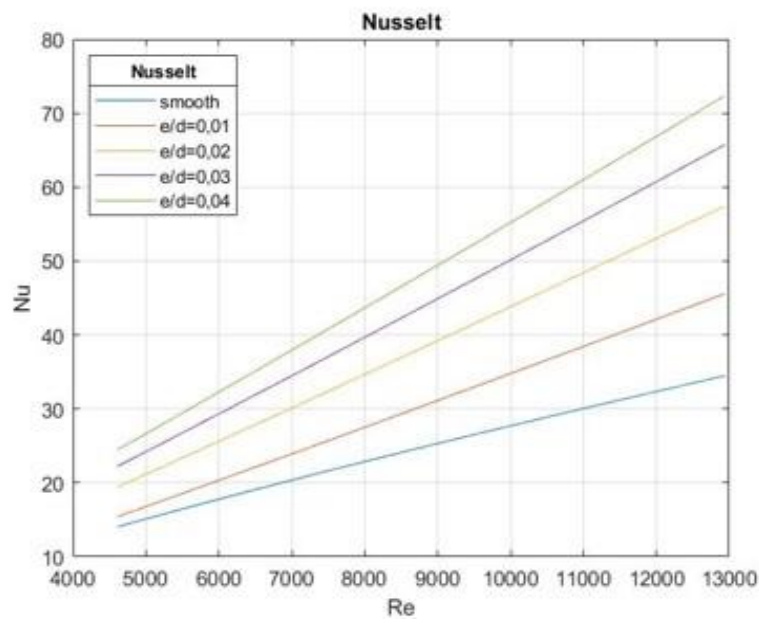


Figure 3.12 - Effect of rib height on Nusselt number

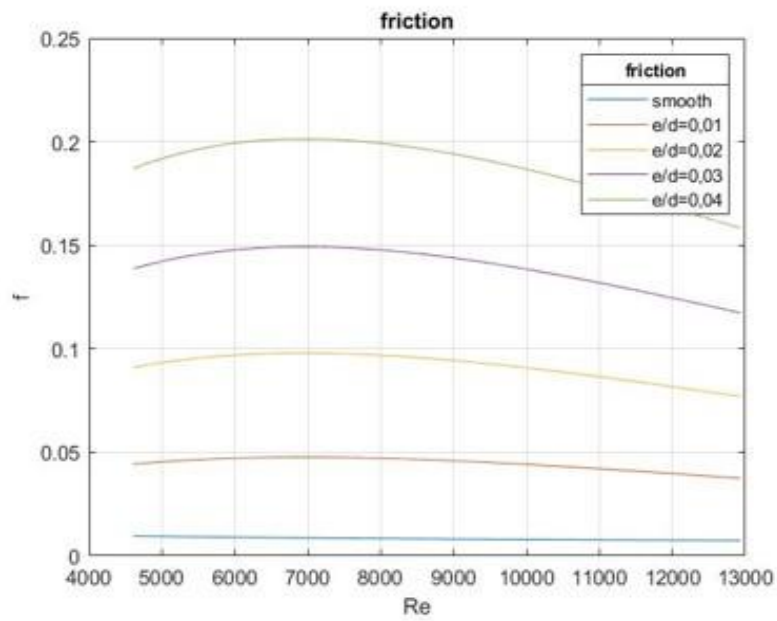


Figure 3.13 - Effect of rib height on friction factor

Finally, after having compared with the latter, the *best case* occurs for values of the ratios equal to:

- $\frac{e}{D} = 0,01$
- $\frac{p}{e} = 10$

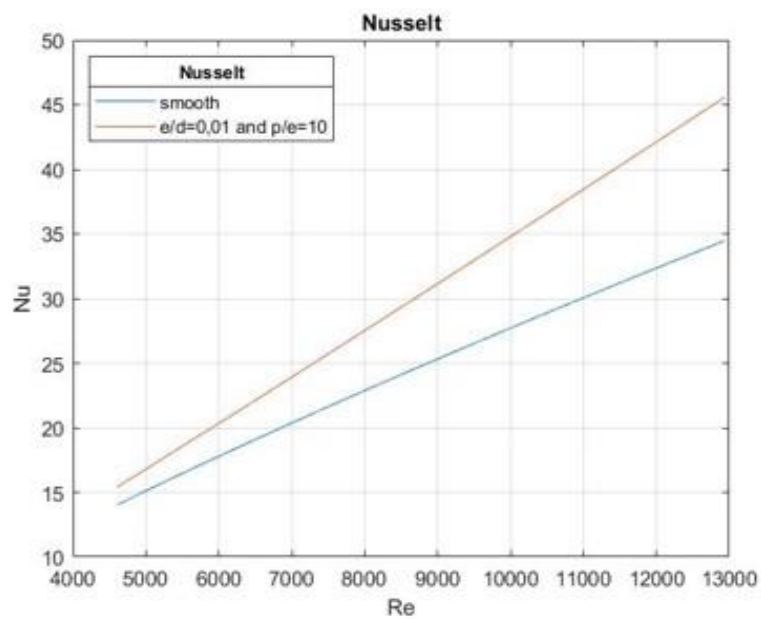


Figure 3.14 - Optimal case for semicircular ribs in terms of Nusselt number

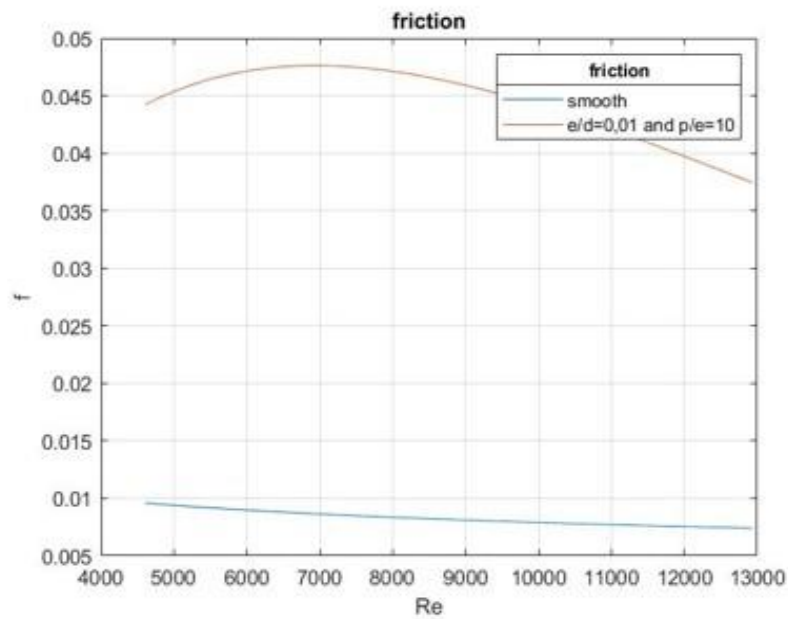


Figure 3.15 - Optimal case for semicircular ribs in terms of friction factor

- Nusselt shows a maximum increase of 32,2% at $Re = 12936$
- The friction coefficient f shows a strong increment, even though the trend tends to decrease at high Re

3.3 Final considerations

Actually, even other two configurations have been validated and solved for optimal, it took as reference studies conducted by Gee and Webb [6] and Han [7]. They were considered mostly for the work that Gee and Webb dedicated to the study on how the angle of attack influenced the fluid flow characteristics, while regarding the study by Han, was worth due to how he increased the attention to this field, his studies were crucial for the development of the rib-roughened channels cooling. In particular, the study subject of this validation concerned trapezoidal shaped ribs, so it would have been really interesting to compare with these other rib geometries. The limit of the correlations developed experimentally were due to the nature of channels in which tests were made; as a matter of fact they were conducted into two parallel plates and so geometric parameters influencing the flow were different with respect to circular channels and the possibility of considering a hydraulic diameter was not enough to put them on the same scale.

Having said that, the two chosen configurations were finally compared in order to have an idea of the actual potential of each of them from the point of view of heat transfer exchange enhancement. Since the studies used for testing different ranges of Reynolds number, the results were scaled in a common range with the purpose to make coherent comparisons. In the following pictures are plotted curves for both Nusselt number and friction factor, as well as it has been done for each configuration before; of course, they concern only the optimal case respectively for rectangular, helical and semicircular ribs.

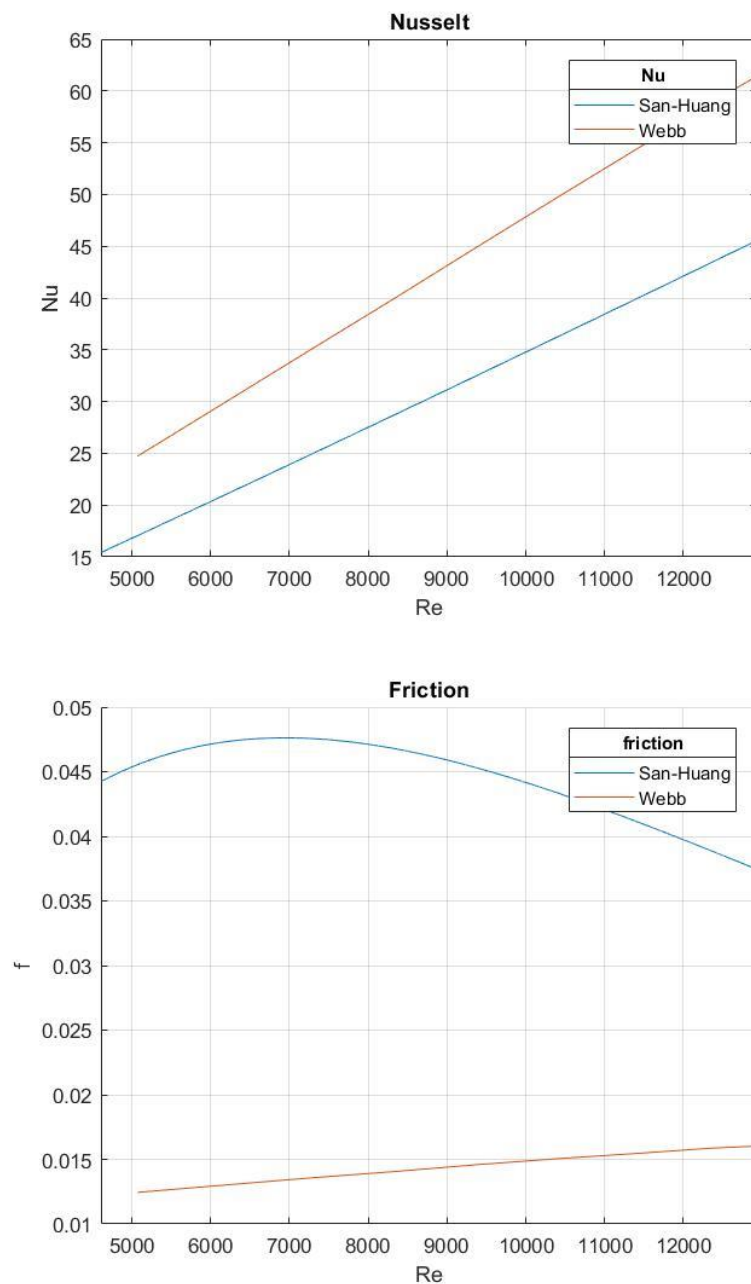


Figure 3.8 - Solutions comparison in terms of Nusselt number and friction factor

All studies confirm $p/e = 10$ as the optimal pitch to height ratio. The rib height has a stronger effect on the friction than on the Nusselt coefficient, so a small value like $e/D = 0,01$ can be used not penalizing too much the thermal performances.

The validation of the correlations, from a mathematical point of view, together with the optimal pursuit for each case was just the starting point of the analysis. As a matter of fact, the prediction made by correlations needed to be verified making fluid dynamics computations through simulations with a given software. Thus, Star CCM+ has been useful for this purpose. In the following chapter will be clear how the models have been implemented in the software and the setting criteria used in order to achieve the wanted results.

Chapter 4

4. Star-CCM+ and mathematical model

4.1 Governing equations

An overview of equations describing fluid motion will be presented in this chapter. Before going through the conservation equations which allow to define the fluid flow characteristics, the mathematical approach exploited by means of total derivative should be defined:

$$\frac{Dx}{Dt} = \frac{\partial x}{\partial t} + \mathbf{u} \cdot \nabla x \quad (4.1)$$

It allows to evaluate the variation of a generic quantity x during time and through space.

4.1.1 Continuity equation

It gives a mathematical description of transport phenomenon, it is the simplest one and very powerful when applied to conservative quantities:

$$\frac{\partial \rho}{\partial t} + \nabla \cdot (\rho \mathbf{u}) = 0 \quad (4.2)$$

Where ρ and \mathbf{u} are respectively fluid density and velocity. For compressible fluid the density represents an unknown and depends on both time and space, contrariwise for incompressible it is known and constant.

4.1.2 Momentum equation

It is the following:

$$\rho \frac{D\mathbf{u}}{Dt} = -\nabla p + \rho \mathbf{g} + \nabla \cdot [\mu(\nabla \mathbf{u} + (\nabla \mathbf{u})^T)] + \nabla \cdot [\lambda(\nabla \cdot \mathbf{u})\mathbf{I}] \quad (4.3)$$

First term on left hand side of the equation is the total acceleration of the fluid; on right hand side there are pressure and gravitational forces ($-\nabla p + \rho \mathbf{g}$) while the last two terms represent the stress tensor: μ is the shear viscosity, it measures the resistance of deformation by stresses, λ is the

volume viscosity and is the fluid resistance to volume expansion, neglected in case of incompressible fluids.

4.1.3 Energy equation

$$\rho \frac{Dh}{Dt} = \frac{Dp}{Dt} + \nabla \cdot (k\nabla T) + \Phi \quad (4.4)$$

With $h = c_p T + p/\rho$ being the specific enthalpy, T is the temperature and k the thermal conductivity of the fluid.

On left hand side of the equation represents the total rate of change of enthalpy, while at right hand side there is the work done by pressure $\left(\frac{Dp}{Dt}\right)$, the conductive heat exchange within the fluid $(\nabla \cdot (k\nabla T))$ and finally the dissipation rate of work done by viscous forces.

The flow is completely defined by these three equations when incompressible, constant density; things change when the fluid is compressible. Another equation needs to be used, such as the equation of state:

$$p = \rho RT \quad (4.5)$$

With R being the specific gas constant.

4.2 Turbulence modelling

In the previous chapter was made explicit that in order to have an augmentation in terms of heat transfer turbulence needs to be triggered. Turbulence as it stands is one of the most unpredictable phenomena, a turbulent regime refers to irregular flows where eddies and flow instabilities occur. Turbulence motion has been experimentally related to the Reynolds number. The latter is defined as the ratio between inertia forces and viscous forces. Whenever inertia forces overcome the viscous forces, instabilities arise and turbulence occurs; more specifically, turbulence regime is established when the Reynolds number exceeds the threshold of laminar flow.

4.2.1 RANS equations

Generally, turbulence should be easily modelled by Navier-Stokes equations, but the problem occurs at high Reynolds number. Due to the aleatory nature of the phenomenon the resolution of the Navier-Stokes equations become really difficult and unstable as well. At high Reynolds

number even slightly varying boundary or initial condition can influence the final result too much. So, the problem is faced by means of the Reynolds-Averaged Navier-Stokes equations.

These new set of equations derive from the already known Navier-Stokes equations, the principle is to consider the mean stream and so all the quantities are time averaged in order to have a good approximation of what actually happens in the fluid flow. The solution basically has a statistic meaning more than a physic one.

Taking velocity as a reference function, consider the mean value as:

$$U_i = \lim_{t \rightarrow \infty} \frac{1}{T} \int_t^{t+T} u \, dt \quad (4.6)$$

Therefore, velocity is decomposed as:

$$u_i = U_i + u'_i \quad (4.7)$$

Where U is the mean velocity while u' corresponds to the fluctuation. This can be extended to all the variables, more generally it is:

$$\phi(\mathbf{x}, t) = \bar{\phi}(\mathbf{x}, t) + \phi'(\mathbf{x}, t) \quad (4.8)$$

As before, $\bar{\phi}(\mathbf{x}, t)$ is the mean value and $\phi'(\mathbf{x}, t)$ is the fluctuation contribution.

The main feature of the fluctuating contribution is that its mean value is equal to zero. Finally, the average Navier-Stokes equations for incompressible flow will be the following:

$$\nabla \cdot \mathbf{u} = 0 \quad (4.9)$$

$$\rho \frac{\partial(\bar{u})}{\partial t} + \rho \nabla \cdot (\bar{u} \times \bar{u} + \bar{u}' \times \bar{u}') + \nabla \bar{p} = \nabla \cdot \bar{\Pi}_v + \rho \bar{a} \quad (4.10)$$

$$\rho \frac{\partial \bar{h}}{\partial t} + \rho \nabla \cdot (\bar{h} \bar{u} + \bar{h}' \bar{u}' - k \nabla \bar{T}) = \frac{\partial \bar{p}}{\partial t} + \nabla \cdot (\bar{\Pi}_v \cdot \bar{u}) \quad (4.11)$$

$\rho \nabla \cdot (\overline{u' \times u'})$ is the Reynolds stress tensor, it accounts for fluctuations in the momentum equation.

Turbulent flows are significantly affected by the presence of walls, where the viscosity-affected regions have large gradients in the solution variables, thus, an accurate presentation of the near wall region determines successful prediction of wall bounded turbulent flows. A strategy using the computed wall y^+ is recommended when dealing with such flows.

Near-wall regions have larger gradients in the solution variables, and momentum and other scalar transports strongly occur. From the Figure [4.1] can be observed that the viscosity-affected region (the inner layer in this case) is made up of three zones (with their corresponding wall y^+), namely the:

- Viscous sublayer ($y^+ \leq 5$)
- Blending region ($5 < y^+ \leq 30$)
- Fully turbulent region ($y^+ > 30$)

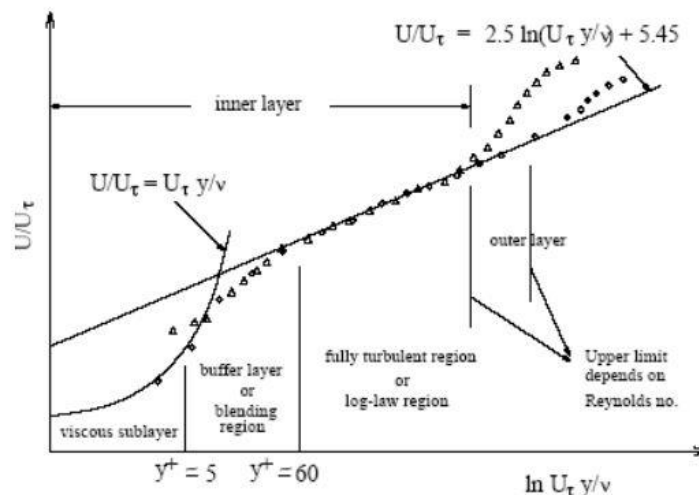


Figure 4.1 - Subdivision Near-wall region

The wall y^+ is a non-dimensional distance similar to local Reynolds number, often used in CFD to describe how coarse or fine a mesh is for a particular flow. It is the ratio between the turbulent and laminar influences in a cell. Very close to the wall, viscous damping reduces the tangential velocity fluctuations, while kinematic blocking reduces the normal fluctuations. Towards the outer part of the near-wall region, however, the turbulence is rapidly augmented by the production of turbulent kinetic energy due to the large gradients in mean velocity. Accurate presentation of the flow in the near-wall region determines successful prediction of wall-bounded turbulent flows.

Values of y^+ close to the lower bound ($y^+ \approx 30$) are most desirable for wall functions whereas $y^+ \approx 1$ are most desirable for near-wall modelling.

The latter is the one this study is interested to model, for this as a turbulence model one between SST Menter $k-\omega$ and Wilcox $k-\omega$ should be chosen. Actually, the first was developed by Boeing to simulate the behaviour of near-wall turbulence flow for external surfaces of planes, while the latter resulted to have a good approach in the vicinity of wall generally. Both of them will be used to see which fits best.

4.3 Preprocessing

From now on there will be a direct comparison between experimental models from articles and the problem reduction faced through Computational Fluid Dynamic (CFD) analysis. The analysis will allow to perform the actual conditions of the fluid flow within given channels, imposing the relative boundary conditions for each surface with the aim at reproducing the experiments already done by Webb, Eckert and Goldstein for rectangular ribs channels and by San and Huang for semicircular ribs channels.

The analysis was conducted on both geometries in parallel, but just to well introduce each problem they will be now addressed singularly.

4.3.1 Rectangular ribs problem – 3D Geometry

Since tests were carried out on different geometries, to perform fluid dynamic analysis only one needed to be chosen. For this, was found a good trade-off by evaluating heat transfer and friction parameters on a channel with rib height-to-diameter ratio equal to 0,01 and rib pitch-to-height ratio equal to 10. This case represented not only one of the geometries tested by Webb et al. but even the optimal case for the rectangular rib correlations, in terms of heat transfer. Summing up:

- $\frac{e}{D} = 0,01$
- $\frac{p}{e} = 10$

Before going through the validation there was a preliminary phase of problem reduction, due mainly to the difficulties of implementing in the software that kind of geometry. Basically, the tested channels from the paper were way too large and with a very high number of ribs. Thus, the problem was reduced to a channel showing only a limited number of ribs allowing the flow to reach fully developed conditions so the evaluation of parameters could have been coherent.

<i>Rectangular ribs</i>	Experimental program	CFD analysis
Channel length [m]	1,52	0,44196
Entrance length (smooth) [m]	0,91	0,18415
Exit length [m]	0,76	0,7366

N° of ribs [/]	412	18
Diameter [mm]	36,83	36,83
Rib height [mm]	0,3683	0,3683
Rib pitch [mm]	3,683	3,683
Rib width [mm]	0,38	0,38

Table 1 - 3D geometry for rectangular ribs configuration

The channel already described has been generated as a 3D solid with SolidWorks. Thus, it is converted into an IGES file and then imported into Star CCM+ with the circled command.

The imported file will be visualized on the lateral bar as a Part geometry:

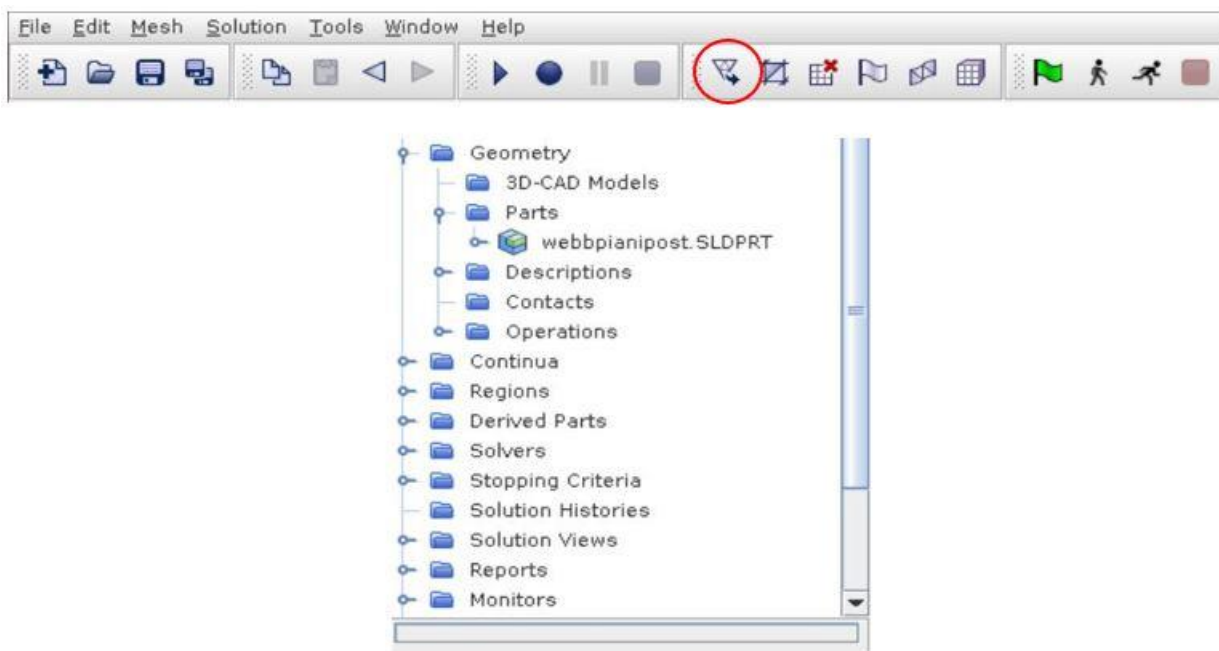


Figure 4.2 - StarCCM+ command bars

Then, surfaces belonging to the solid need to be divided in order to allow lately to set the boundary conditions for each Part surface.

4.3.2 Semicircular ribs problem – 3D Geometry

For what regards the semicircular ribs case, the technique is exploited starting from the publication of the studies conducted by San and Huang (2006). The configuration to be tested with CFD had as geometric parameters the following:

- $\frac{e}{d} = 0,015$
- $\frac{p}{d} = 0,75$

In this case there was not the possibility to exploit directly the optimal value found from correlations in Matlab. For the same reasons as before, in this case the problem was reduced to perform the analysis:

<i>Semicircular ribs</i>	Experimental program	CFD analysis
Channel length [m]	1,52	0,2068
Entrance length (smooth) [m]	Not specified	/
Exit length [m]	Not specified	/
N° of ribs [/]	147	15
Diameter [mm]	13,8	13,8
Rib height [mm]	0,206	0,206
Rib pitch [mm]	10,34	10,34
Rib width [mm]	2	2

Table 2 - 3D geometry for semicircular ribs configuration

An entrance and exit length has not been imposed for this case because, as it will be clear later from the Nusselt number plot, the flow resulted to be fully developed.

4.3.3 Meshing

The meshing problem represents most likely the main feature of this study. From the beginning different meshes have been used for the models in order to find the best trade-off between reliability of results and the need keeping low the number of cells. Since the meshing problem has been faced in the same way for both the configurations, the analysis can continue in parallel just by differencing what are actually the mesh sizes used for each case.

The first step in generating a mesh is to choose the meshing strategy, as Star CCM+ provides two different kinds:

- Parts Based Meshing
- Region Based Meshing

For our analysis Parts Based Meshing has been chosen.

Before going through next steps and generating the mesh for our part, the assignment of parts to region is fundamental to approach the problem by imposing boundary conditions. **Assign parts to regions** is the command which creates a relationship between the meshed part and the physic region.

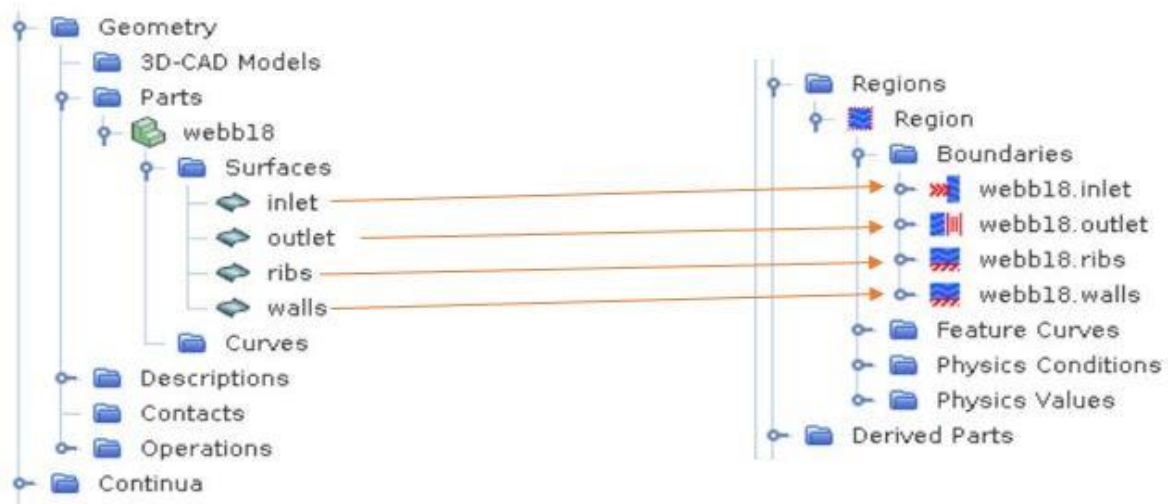


Figure 4.3 - Relationship between Part geometry and Regions

Surface and volume meshing

One surface meshing model is provided:

- The **surface remesher**, always required for geometries imported from CAD models or generated as 3D-CAD.

As concerns volume meshing, the models used for this work are:

- **Polyhedral mesher**, suited for multi-part geometries.
- **Prism layer mesher**, combined with the previous allows prism cells next to wall, essential for turbulent flows.

- **Generalized cylinder mesher**, used specifically for our geometry, being a circular channel.

Meshing model settings and sizes

Before mesh generating could happens, settings must be changed according to the quantities that need to be analysed. Below, are listed the refinements applied for each case:

	Rectangular ribs	Semicircular ribs
Base size [mm]	2	2
Number of prism layer [/]	15	15
Prism layer stretching [/]	1.5	1.5
Prism layer total thickness [% of Base size]	10	10

Table 3 - Mesh settings for both cases

A custom control is then applied to the rib surfaces with a Target Surface Size equal to $2e^{-4}$ m.



Figure 4.4 - Mesh on 3D geometry with rectangular ribs



Figure 4.5 - Mesh on 3D geometry with semicircular ribs

	Rectangular ribs channel	Semicircular ribs channel
Number of cells	998.906	987.176

Table 4 - Number of cells in 3D mesh

4.3.4 Continua and regions

Continua and regions are used together to catch the physical and material properties of a model.

A *continuum* represents a material in combination with a set of physics models that will be used to simulate the response of the material to the conditions imposed upon it. A continuum also provides the facility to define reference and initial values.

Instead, a *region*, represents one or more volumes within the overall model which will share the same continuum and set of boundary conditions. As showed before, regions are recognized and defined from CAD parts.

Among continua, regions, boundary conditions and CAD parts holds a very strong relationship. To give a correct understanding of the matter, a series of implicit constraints is listed below:

- Each region should be associated with a continuum
- More than one region could be associated with the same continuum
- Boundary conditions belong to regions, without the possibility to be shared between regions
- Every CAD surface must be associated with a given boundary condition

Using a physics continuum is essential to identify the problem and set which are the solutions that the software will go to find when simulating. Therefore, a correct choose of models within the continuum will permit a well defined resolution of the problem. In all analysis of this work, the following physics models have been chosen:

- Space: *Three Dimensional*
- Time: *Steady*
- Material: *Gas*
- Flow: *Coupled Flow*
- Equation of state: *Ideal Gas*
- Viscous Regime: *Turbulent*
- Turbulence: *K- ω Turbulence*
- K- ω Turbulence: *SST Menter K- ω*
- K- ω Wall Treatment: *Low y^+ Wall Treatment*

Concerning material properties of the gas, fundamental hypothesis in the model, are listed in the table below:

<i>Fluid</i>	
μ , Dynamic Viscosity [m^2/s]	Constant
c_p , Specific Heat [$J/kg \cdot K$]	Constant
λ , Thermal Conductivity [$W/m \cdot K$]	Constant
<i>Models</i>	
Coupled Flow Discretization	2 nd order
K- ω Convection	2 nd order

Table 5 - Fluid (air) properties

Boundary conditions

A brief introduction of boundaries which have been used in the model is useful to understand how the program will recognize each of them. Later, an overview of the boundaries chosen to perform experimental procedure will be done together with the associated settings in the model.

- **Velocity Inlet:** in Star CCM+ the surface normal inlet velocity is directly specified. The relative boundary pressure is evaluated automatically by means of reconstruction gradients.
- **Pressure Outlet:** specify the gauge pressure at the outlet. Again, face velocity is extrapolated using reconstruction gradients from the adjacent cells.
- **Wall:** with this boundary the tangential velocity is set to zero. No velocities are present in a boundary used as wall.

At the wall is possible to impose conditions such as a Constant Temperature or an Heat Flux.

Here, is necessary to compare boundaries from the studies taken as references and the ones implemented in the model. In first analysis, as was anticipated, having two different ranges of Reynolds number testing for the two experiments, the validations will be performed for different values of the number as well:

- Reynolds number for rectangular ribs: 100.000
- Reynolds number for semicircular ribs: 12.000

For each Reynolds number are evaluated the velocities which will be used as inlet boundary conditions:

$$Re = \frac{\rho v_{ave} \cdot D}{\mu} \quad (4.12)$$

$$\dot{m} = \frac{\mu \cdot \pi D \cdot Re}{4} \quad (4.13)$$

$$v_{ave} = \frac{\dot{m}}{\rho \cdot \frac{\pi D^2}{4}} \quad (4.14)$$

Regarding the other boundaries, from the papers (of both Webb et al. and San et al.) some information is not given. For instance, for the semicircular ribs case, it is specified that the part of the channel which is tested is kept in a water tank allowing to impose a Constant Temperature at the walls, but the temperature is actually not specified; while a totally different situation holds for the rectangular ribs case, as a matter of fact in that study there is no explanation about the conditions in which the tested tube walls are maintained, as a first approximation will be imposed a Constant Temperature equal to the semicircular ribs case. Attempts should be done to find which were actually the boundaries accounting for those results.

In the following table are listed the boundaries imposed to each part surface, for the Wall boundary conditions an underline will be fixed to remind the uncertainty of the values.

Rectangular ribs			
<i>Part region</i>		<i>Experimental procedure</i>	<i>CFD analysis</i>
Inlet	Velocity inlet [<i>m/s</i>]	40,16	40,16
Outlet	Pressure outlet [<i>Pa</i>]	0	0
Wall	Constant Temperature [<i>K</i>]	<u>343,15</u>	<u>343,15</u>

Table 6 - Boundary conditions imposed for rectangular rib geometry

Semicircular ribs			
<i>Part region</i>		<i>Experimental procedure</i>	<i>CFD analysis</i>
Inlet	Velocity inlet [m/s]	12,86	12,86
Outlet	Pressure outlet [Pa]	0	0
Wall	Constant Temperature [K]	<u>343,15</u>	<u>343,15</u>

Table 7 - Boundary conditions imposed for semicircular rib geometry

This first analysis has the goal to show if and how the mesh definition could prejudice the model validation. For this, a low number of cells is present if compared to the actual volume of each case. The resulted meshes, as it is clear from the pictures, look very coarse not only in the mid portion of the volume but actually in the neighbourhood of the ribs as well.

4.4 Postprocessing

Star CCM+ gives the possibility to create plots and scenes to see how the interesting parameters change at the end of each simulation when the stopping criteria is satisfied. Precisely, all the simulation were launched with a stopping criteria equal to 10.000 iterations. Recalling, in scenes and plots it is mandatory to choose among the field function to see its variation.

In this thesis the following scenes and plots were used to obtain graphical results:

- Scalar scene for temperature profile
- Scalar scene for velocity profile
- Vector scene for velocity profile
- Plot of Nusselt Number as a *Field function*

Even the section Report has been useful to evaluate Absolute Total Pressure in a specific section of the model as well as the Bulk Temperature, respectively needed to identify the Pressure drop and the Mean Nusselt number.

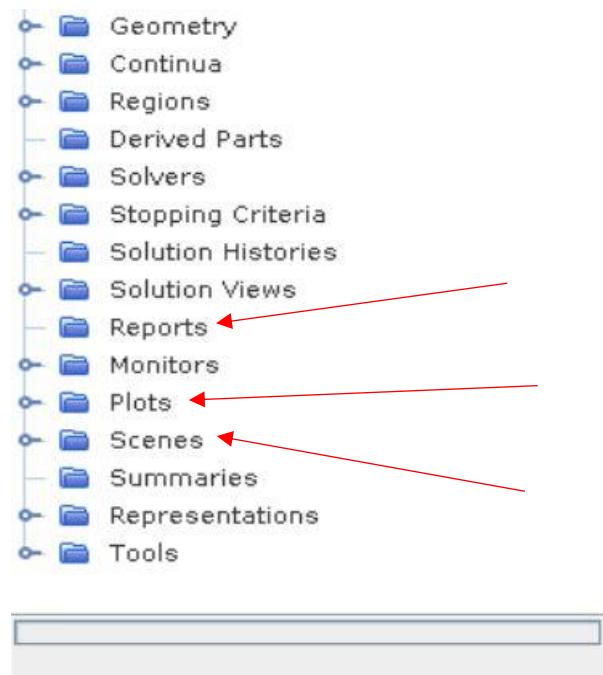


Figure 4.6 - StarCCM+ functions bar

4.5 Results comparison

Therefore, results from simulations needs to be compared to that expected from experimental analyses and correlations. As said before they should be compared from the point of view of Nusselt number and Friction factor.

It is worth to comment firstly results regarding the rectangular ribs channel. In order to simplify this part of the work, comparing the Nusselt number values seems to be enough to say that a mesh like the one presented before would never fit to this case of study, because the actual phenomena of separation and reattachment occurring in correspondence of the ribs will need a thicken of the mesh itself to describe the part.

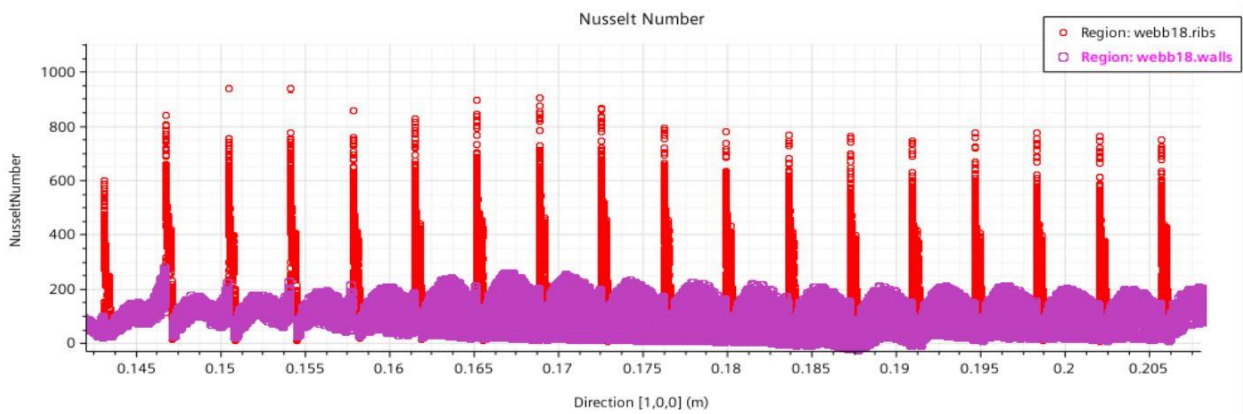


Figure 4.7 - Nusselt trend for 3D geometry with rectangular ribs

The plot is obtained by imposing in the *Field function* section the values related to this case for the Nusselt number, which are:

- Bulk Temperature: 296,30 K (evaluated by performing a Mass Flow Averaged in Reports for a section within the ribbed wall)
- Relative Length (Diameter): 36,83 mm
- Conductivity coefficient: 0,0257 W/mK

It is worth to say that from the plot of Figure [4.7] the flow results not to be fully developed, so an higher entrance was needed.

Again, vortexes which should appear between ribs are not defined with this approach. Only the separation is here visible but the effect related to, such as vortex generation are totally neglected with this mesh settings.

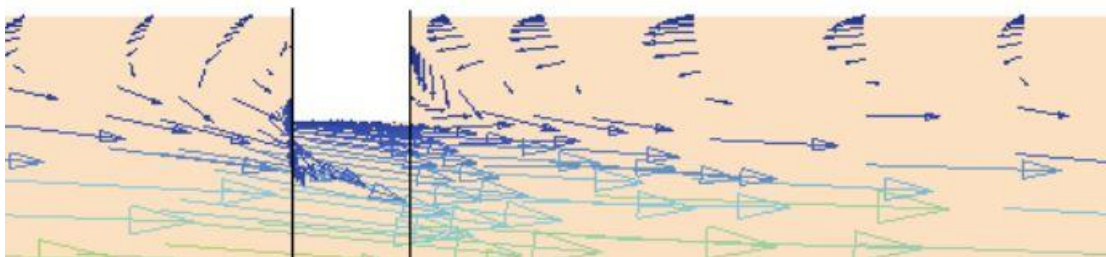


Figure 4.8 - Vector scene for velocity

Rectangular ribs channel			
Parameter	Experimental procedure	Correlation	CFD
Nusselt number	386	376,3	120,04

Table 8 - Nusselt number comparison among different methods

The results in terms of Nusselt number are too far away from the correct solution. Thus, a new approach needs to be applied to the case in order to get the validation.

On the other hand, for the semicircular ribs case the solution looks different. As a matter of fact, in this case all the previously mentioned phenomena occurring nearby the ribs are less marked with respect to the rectangular ribs channel. Since separation does not occur due to the low height of the rib, the effects of a strong reattachment disappear. For this, results seem to be more coherent even with a very coarse mesh.

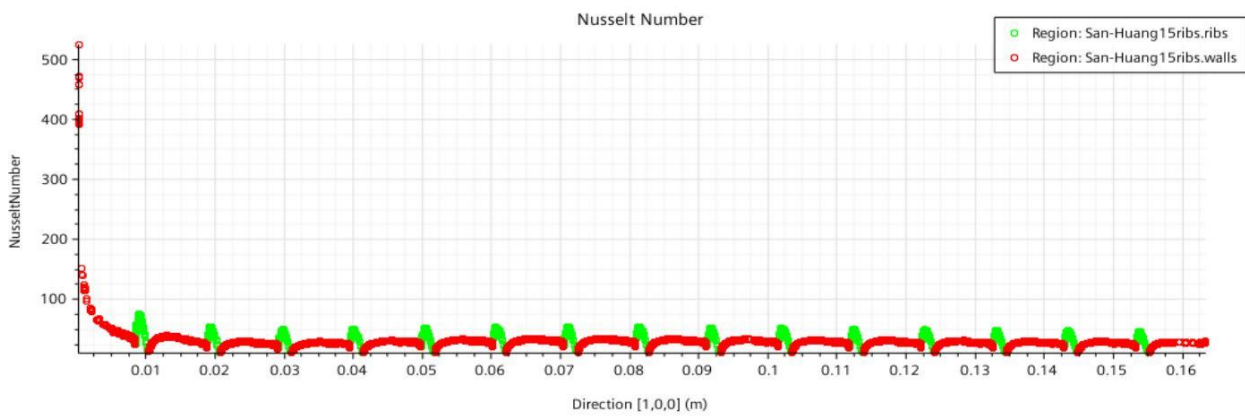


Figure 4.9 - Nusselt trend for 3D geometry with semicircular ribs

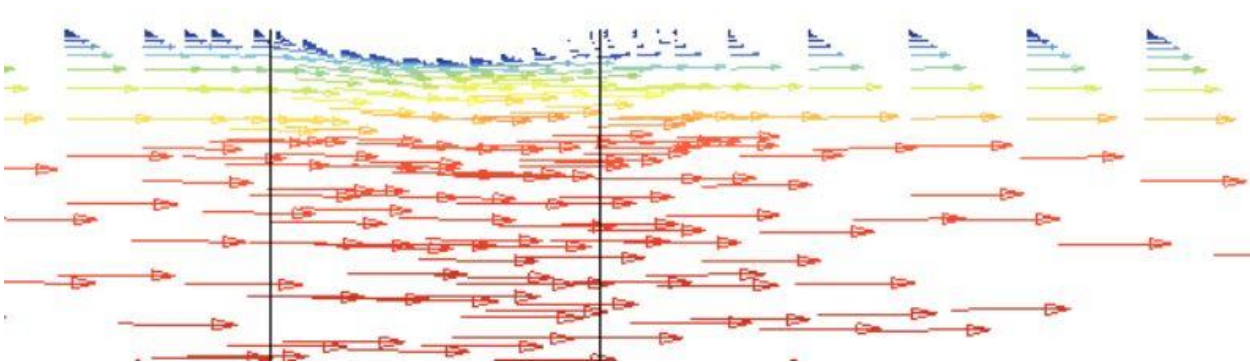


Figure 4.10 - Vector scene for velocity

Following, a table with Nusselt number comparison is shown:

Semicircular ribs channel			
<i>Parameter</i>	Experimental procedure	Correlation	CFD
Nusselt number	36,42	35,63	30,96

Table 9 - Nusselt number comparison among different methods

4.5.1 Turbulence discussion

After having evaluated the Nusselt number is clear that the previous mentioned turbulence model such as SST Menter $K-\omega$, does not fit good for our case. So, another method is selected for a new simulation, which is the **Standard (Wilcox) $K-\omega$** .

More coherent results are obtained by using this turbulence model and for this, it is used even for further analyses. To give an idea a table will show the new results. It will be clear that in the semicircular ribs case they look very close to the experimental given by San et al., while for the rectangular ribs the result seems to be still so far away.

Nusselt Number	Rectangular ribs	Semicircular ribs
Experimental procedure	386	36,42
Correlation	376,3	35,63
SST Menter $K-\omega$	120,4	31,10
Standard (Wilcox) $K-\omega$	160,63	36,03

Table 10 - Evaluation of Nusselt number with different models and comparison

4.5.2 Mesh refinement

In order to find the wanted results the previously presented mesh sizes were reduced, ending up with a really fine mesh counting for both cases about 7 million cells. Still, for the semicircular ribs case the result was coherent with the previous; instead, for the rectangular ones a step closer was done. At this point the study seemed to be near to a solution, achieved by just increasing the number of cells within the channel. Unfortunately, the latter simulation performed with that high

number of cells (almost 7 million) shown a computation time too high, near to 17 hours. A solution to avoid this problem will be presented in the next chapter.

5. Models Validation

The problem as it is presented is axisymmetric. The problems in which the body possesses a symmetry axis and the boundary conditions and other parameters of the problem are symmetric with respect to this axis are called as axisymmetric problems, this means that a different approach could be chosen reducing it to a 2D study. Fortunately, Star CCM+ allows to set a problem to a 2D geometry and to perform simulations. In this way, the number of cells which define the domain can be enhanced to describe properly the Part geometry. Actually, the advantages presented by simulating this kind of domain are multiple, starting from the computational time to the mesh definition properties. The reduction to a 2D domain could be performed only to the case with rectangular ribs, instead it is extended to the semicircular case even if the simulation with the previous mesh shown a good trend, and results were well approximated with the correlations, with the aim at carrying out a coherent work.

5.1 Domain reduction: 2D

Always with the help of SolidWorks the geometry is now defined by a 2D shape, a small thickness needs to be applied in order to let the software reading the IGES file. The domain to be read and solved in Star CCM+ should be generated in the YZ plane, with X being the axis of symmetry of the part. The tables below provide geometric values for both channels:

	Rectangular ribs		Semicircular ribs	
	Experimental program	CFD analysis	Experimental program	CFD analysis
Channel length [m]	1,52	0,44196	1,52	0,4828
Entrance length (smooth) [m]	0,91	0,3683	Not specified	0,138
Exit length [m]	0,76	0,3683	Not specified	0,138
N° of ribs [/]	412	20	147	20
Diameter [mm]	36,83	36,83	13,8	13,8
Rib height [mm]	0,3683	0,3683	0,206	0,206
Rib pitch [mm]	3,683	3,683	10,34	10,34
Rib width [mm]	0,38	0,38	2	2

Table 11 - 2D geometry adopted for axisymmetric case

In the following pictures are presented the two new CAD models in 2D:

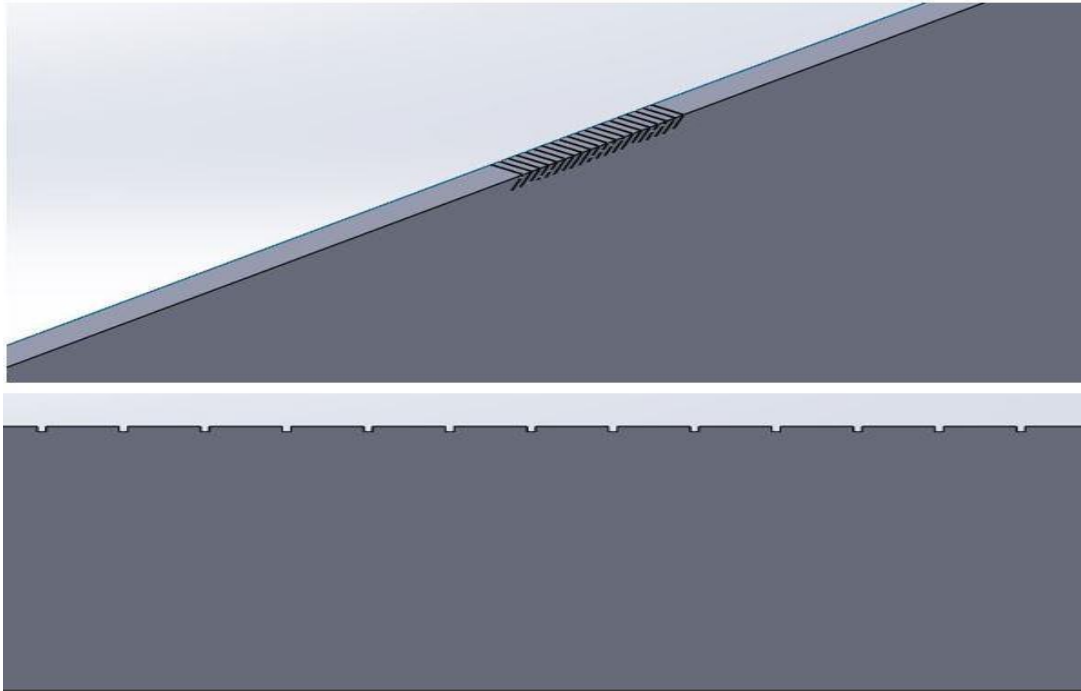


Figure 5.1 - Rectangular ribs CAD - 3D view (top) and lateral view (bottom)

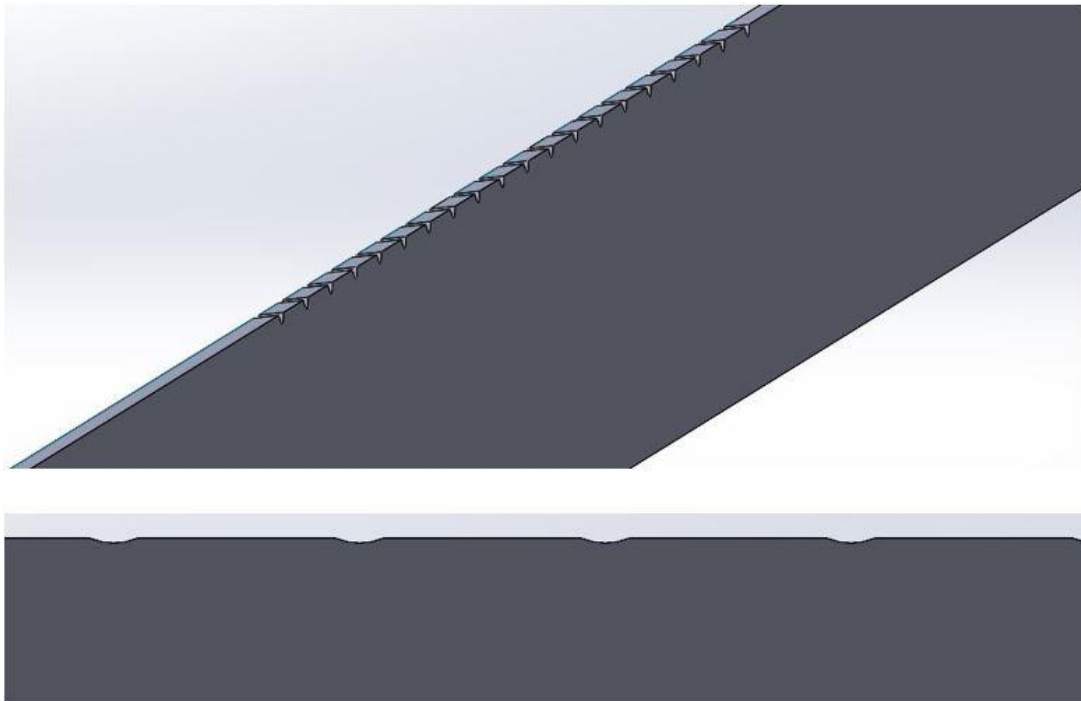


Figure 5.2 - Semicircular ribs CAD - 3D view (top) and lateral view (down)

Now, being the whole domain infinitely smaller with respect to the previous presented 3D cylinder, is easy to generate a finer mesh. At this point, the choice was to use a Structured mesh. Since this kind of mesh requires a higher number of cells with respect to the Polyhedral or Tetrahedral ones, it is now the case that this not corresponds to a problem anymore.

5.1.1 Surface division

This step is fundamental in order to set different mesh sizes. In the following pictures are reported the surfaces divided on the lateral side of the component, whose mesh settings will be different.

- Rectangular ribs surface division

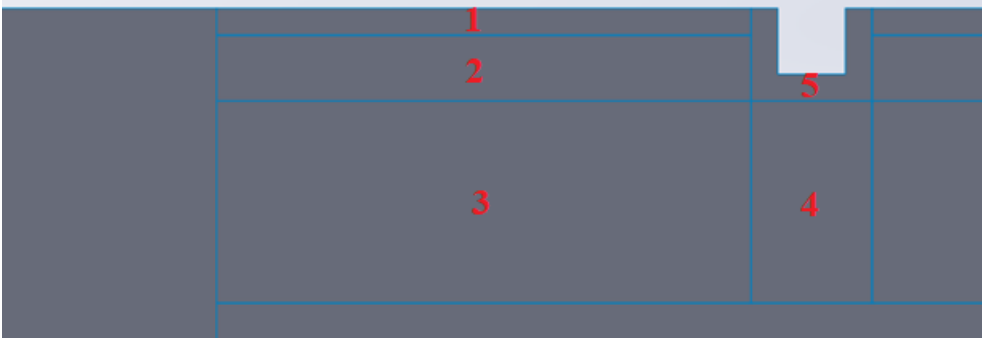


Figure 5.3 – Rectangular ribs surface division

Surfaces are numbered to recall which are the name used in StarCCM+ to define the meshing values:

- 1 – rib source 1
- 2 – top source
- 3 – mid source 1
- 4 – mid source 2
- 5 – rib source 2

- Semicircular ribs surface division

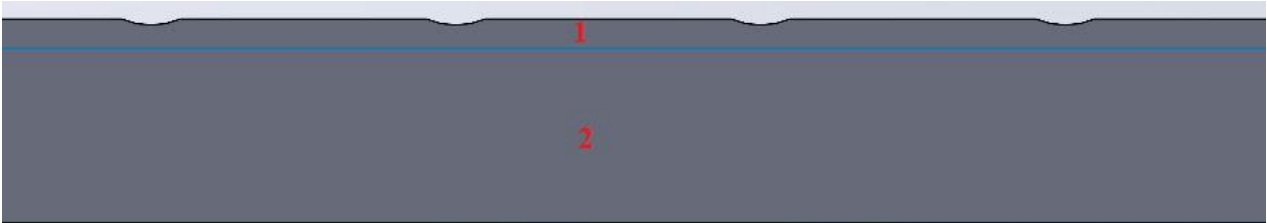


Figure 5.4 - Semicircular ribs surface division

As before, surfaces are numbered, so:

1 – top source

2 – internal source

5.2 Structured Mesh

To perform this operation, as well as before, a Part meshing has been chosen. This kind of mesh could be generated by revolution or extrusion, the latter fitted for our case.

Surface and volume meshing

On StarCCM+ choose a *surface* Directed Mesh operation, thus, Source and Target Surfaces should be specified; the Source Surface is the one to which the mesh settings are applied so an extrusion can be performed till the Target Surface.

After imposing a Directed Mesh, a *volume* mesh should be chosen, therefore, an Automated Mesh operation with the following properties is selected:

- Quadrilateral Mesher
- Prism Layer Mesher

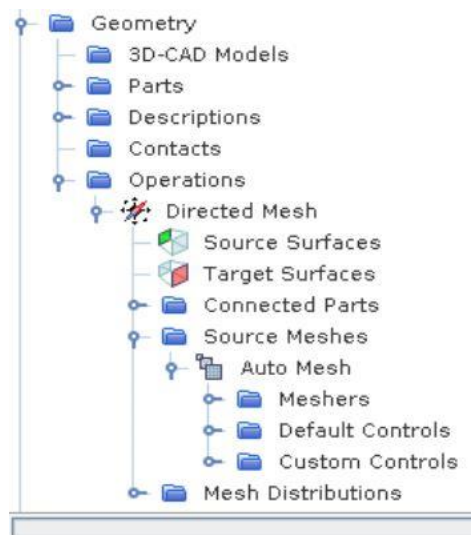


Figure 5.5 - Setting a Directed mesh on StarCCM+

It is now important to see how effectively the change in geometry can help to have such a finer mesh in proximity of ribs while a coarser next to the symmetry axis. As a matter of fact, a custom

control is applied to the surfaces generated on the lateral surface of the CAD model, allowing to choose different meshing values to end up with the wanted result.

Mesh settings

In the following table are listed the values of the sizes used to generate the mesh. Two different tables will be necessary because each case has different rib geometry and then a different surface division. For rectangular ribs:

		Rectangular ribs
General settings		
	Base size	2 mm
	Number of Prism Layer	20
	Prism Layer Stretching	1.2
	Prism Layer Total Thickness	2% of Base size
Custom control on top source – rib source 1 – rib source 2 – mid source 1 – mid source 2		
	Target Surface Size	2e-5 m
Custom control on internal source		
	Target Surface Size	1 mm
	Minimum Surface Size	4e-5 m

Table 12 - Meshing values used for structured mesh in rectangular ribs geometry

Therefore, an overview of the resulted mesh is given by the following images:

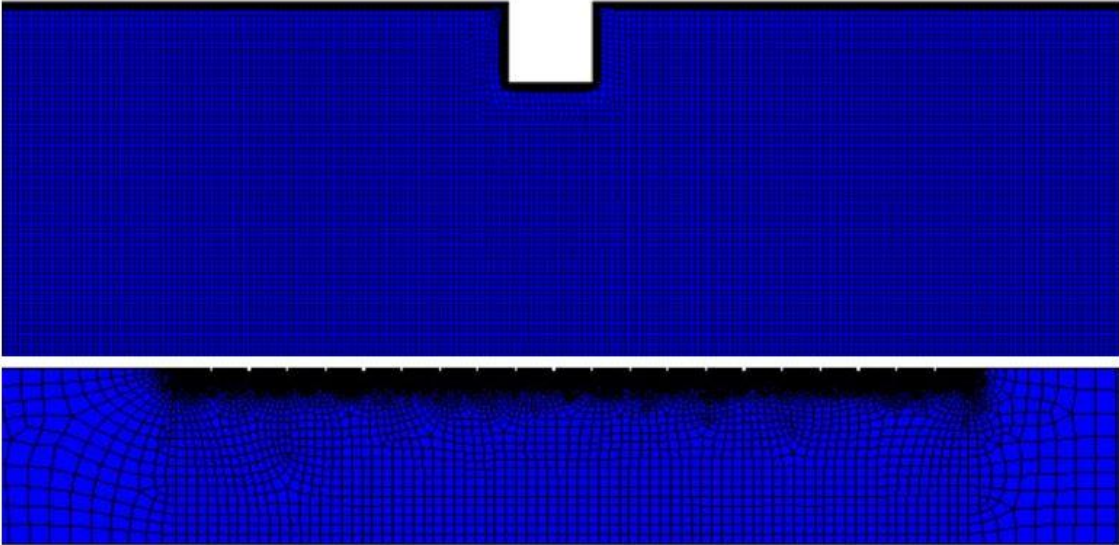


Figure 5.6 - Mesh distribution in proximity of ribs (top) and an overview of the whole channel (down)

Mesh properties:

Cells	Vertices	Faces
321.963	641.507	648.588

Table 13 - Mesh properties (rectangular)

From Figure [5.6] is clear that a finer mesh is obtained where it is interesting to understand how the rib geometry influences the fluid flow. Mostly, it is important that a vortex phenomenon is caught, with this mesh refinement could happen easily. Considering that the geometry is now in 2D, more than 321 thousands cells define the whole domain, which is a good result.

For semicircular ribs:

		Rectangular ribs
General settings		
	Base size	2 mm
	Number of Prism Layer	20
	Prism Layer Stretching	1.2
	Prism Layer Total Thickness	2% of Base size
Custom control on top source		
	Target Surface Size	5,5e-5 m
Custom control on internal source		
	Target Surface Size	1 mm

Table 14 - Meshing values used for structured mesh in semicircular ribs geometry

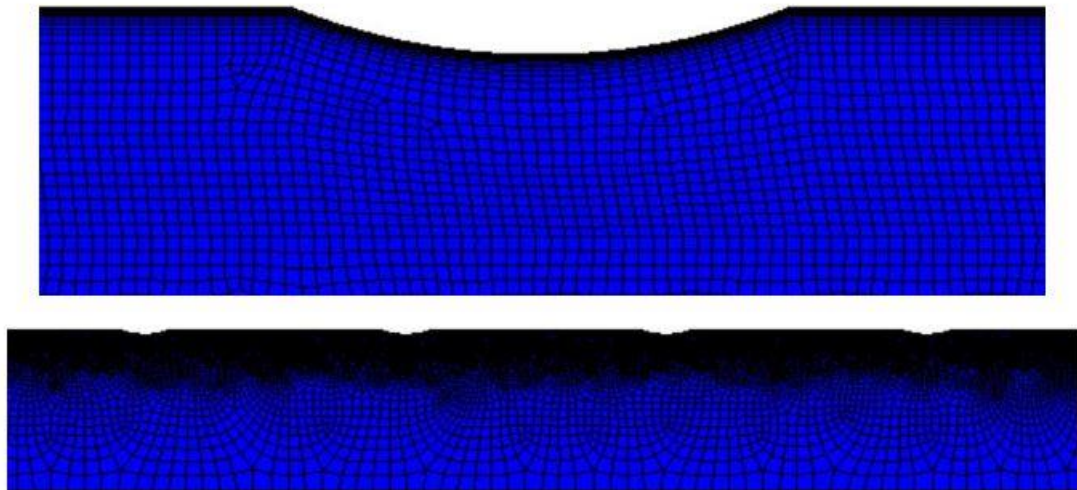


Figure 5.7 - Mesh distribution in proximity of ribs (top) and an overview of the whole channel (down)

Mesh properties:

Cells	Vertices	Faces
458.258	731.525	758.543

Table 15 - Mesh properties (semicircular)

5.3 Validation

This section will show how the validation is carried out, with a following analysis of results and finally a direct comparison between CFD simulation and experiments will be done. First of all, it is worth to recall that, as anticipated in previous chapters, this analysis will be focused on evaluating Nusselt Number, accounting for heat transfer, and friction factor, through pressure losses.

These parameters should be compared and verified, to give a well-defined model, with different boundary conditions. Therefore, simulate the behaviour of such channels at various Reynolds numbers is crucial for the analysis to be considered as coherent. As shown before, the two models taken as references (with rectangular and semicircular ribs) have been tested experimentally for different Reynolds number ranges, namely:

	Rectangular ribs	Semicircular ribs
Range of Re	6.000 ÷ 100.000	4.608 ÷ 12.936

Table 16 - Reynolds number ranges for both geometry experiments

For this, the corresponding Reynolds chosen for each configuration are different, listed below:

Reynolds Number	Rectangular ribs	Semicircular ribs
Case 1	100.000	12.000
Case 2	50.000	8.000
Case 3	20.000	6.000

Table 17 - Reynolds numbers computed in CFD analysis

The parameters which mostly are influenced by the changing Reynolds number are the Velocity as well as the Total Temperature at the Inlet boundary. Further information is given by means of the equations used to evaluate both the parameters:

v_{inlet} from mass-flow rate (equation 4.14)

$$T_{total} = T_{static} + \frac{v^2}{2c_p} \quad (5.1)$$

5.3.1 Physics settings and boundary conditions

The physics set in the *continua* is now connected to a Region 2D, so a different modelling is adopted. Regarding boundary conditions something changed due to the presence of symmetry surfaces having an axisymmetric problem. Here, briefly are reported both the chosen solvers together with the new boundary conditions.

Physics

As anticipated, the following characteristics fit for the new 2D domain:

- Space: *Axisymmetric*
- Time: *Steady*
- Material: *Gas*
- Flow: *Coupled Flow*

- Equation of state: *Ideal Gas*
- Viscous Regime: *Turbulent*
- Turbulence: *K- ω Turbulence*
- K- ω Turbulence: *Standard (Wilcox) K- ω*
- K- ω Wall Treatment: *Low y^+ Wall Treatment*

Boundary Conditions

The following boundary conditions are recalled, being imposed to the new domain:

- **Velocity Inlet**
- **Pressure Outlet**
- **Wall**
- **Axis:** after converting the geometry in 2D it should be specified the axis for which the symmetry is respected.

A new boundary will be imposed to the surfaces which are internal to the domain, belonging to the symmetry axis:

- **Symmetry Plane:** it represents an imaginary plane of symmetry in the simulation. It is used to reduce the extent of the computational domain, where the flow and the geometry are symmetric.



Figure 5.8 - Image from the section Region 2D on StarCCM+

Boundary conditions for both cases are listed below:

<i>Rectangular ribs configuration</i>		Reynolds Number		
Part Surface	Boundary condition	20.000	50.000	100.000
Inlet	Velocity Inlet [m/s]	8,03	20,08	40,16

Outlet	Pressure Outlet [Pa]	0	0	0
Ribbed wall	Wall: Heat Flux [W/m^2]	2500	2500	2500
Entrance+exit walls	Wall: Adiabatic	/	/	/
Side surface	Symmetry Plane	/	/	/

Table 18 - Boundary conditions applied to 2D rectangular ribs geometry

<i>Semicircular ribs configuration</i>		Reynolds Number		
Part Surface	Boundary condition	6.000	8.000	12.000
Inlet	Velocity Inlet [m/s]	6,43	8,57	12,5
Outlet	Pressure Outlet [Pa]	0	0	0
Ribbed wall	Wall: Constant Temperature [K]	343,15	343,15	343,15
Entrance+exit walls	Wall: Adiabatic	/	/	/
Side surface	Symmetry Plane	/	/	/

Table 19 - Boundary conditions applied to 2D semicircular ribs geometry

5.4 Results discussion – Rectangular ribs configuration

As said before, results will be presented in terms of Nusselt Number and friction factor. Since the main goal of this work is to exploit the heat transfer gained with a change in geometry, Nusselt Number will be evaluated first. The Postprocessing is the same as explained in section [4.4], here a brief recap.

The following scenes and plots were used to obtain graphical results:

- Plot of Nusselt Number as a *Field function*
- Scalar scene for temperature profile
- Scalar scene for velocity profile
- Vector scene for velocity profile

The results will be shown for both the configuration with an overview of Plots and scenes generated in StarCCM+, finally they will be presented in tables and even a comparison with literature will be done.

Nusselt Number

Results for this case need to be reported in terms of Stanton number, with a direct correlation holding between the latter and Nusselt number. Thus, a previous evaluation of Nusselt number should be done. The average Nusselt number should be evaluated in the zone where the ribs are present. This can be done by using the Report section in StarCCM+ which allows to evaluate the Surface Average of interesting parameters, in this case Nusselt number.

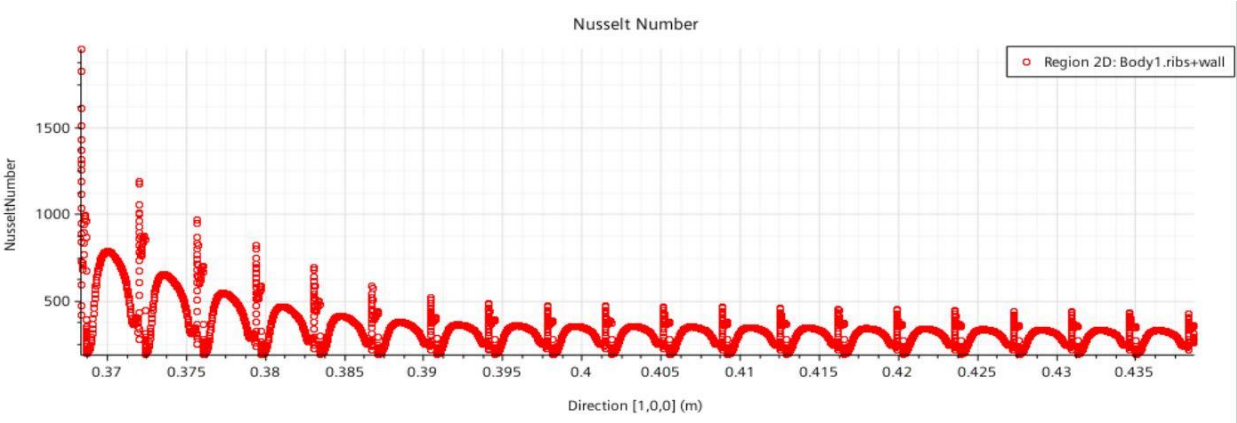


Figure 5.9 - Nusselt number plot from StarCCM+ for rectangular ribs

In the plot above the Nusselt number trend evaluated at each cell of the domain belonging to the ribbed part of the channel. The stabilization of the trend from the sixth rib is clearly depicted, this is fundamental in order to consider validate the simulation. For this, even the flow can be considered fully developed, achieved thanks to an entrance and an exit length long enough to avoid the presence of entrance and outlet disturbances.

Scalar and Vector scenes: Velocity

Later, the velocity should be analysed from both the scalar and vector point of view. The first scene should confirm the dutifulness of the boundary condition applied at the Inlet. An example of it is given in the picture below, by taking as reference the simulation related to a Reynolds number equal to 100.000 and so a velocity of 40,16 m/s.

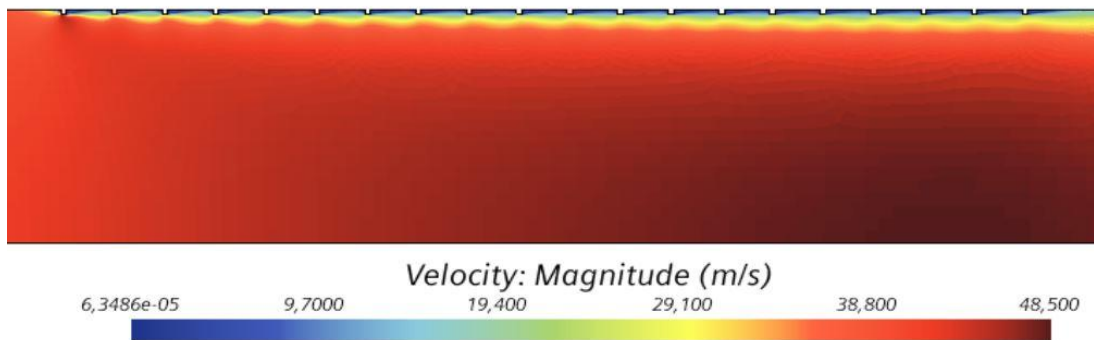


Figure 5.10 – Scalar scene velocity profile for rectangular ribs

Of course, the fluid flow in its path tends to accelerate, the mean velocity is the one that should be respected and is evaluated from a Report in StarCCM+, where is equal to 40,16 m/s.

Instead, a Vector scene is of fundamentally importance because, as introduced before, vortexes can be seen from it. The presence of vortexes will confirm a good mesh definition and of course this phenomenon influence heat transfer characteristics.

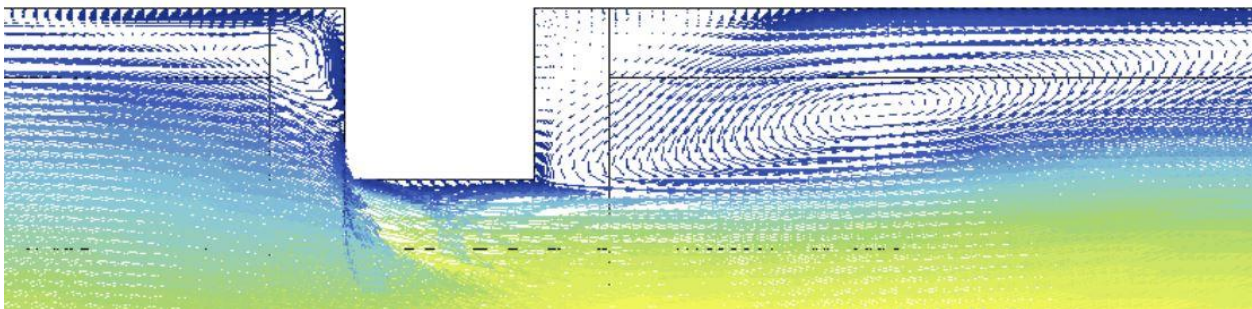


Figure 5.11 - Vector scene velocity profile for rectangular ribs

From the scene above are clearly defined vortexes on both sides of the rib. Vortexes influence even the pressure drop within the channel and corresponds to a corroboration of the presence of separation and reattachment due to the change in geometry.

Pressure drop and friction factor

Following, an analysis of the friction factor is done. The experiments for the evaluation of the friction factor were conducted with Adiabatic walls, so no heat exchange occurred. Another file was simulated for each Reynolds number with a different boundary condition on walls, in order to follow the same procedure.

From the plot above regarding the Nusselt number was clear that a totally developed flow with a stabilization of parameters happened from the sixth rib. So, for the evaluation of pressure drop two sections have been generated in the geometry, one after the sixth rib and the second after the last rib (twentieth). Again, a Report allowed to evaluate the Absolute Total Pressure at each section and by means of the formula (2.3) the friction factor was computed:

$$f = \Delta p \cdot \frac{D}{L} \cdot \frac{2}{\rho v_{ave}^2} \quad (5.2)$$

Where:

Δp [Pa] is the pressure drop between the generated sections

D [m] is the duct diameter

L [m] is the length which passes between the sections

ρ [$\frac{kg}{m^3}$] is the fluid density

v_{ave} [$\frac{m}{s}$] is the mean velocity

Wall y^+

The scalar scene representing the Wall y^+ confirms that the analysis of the flow next to wall is done correctly. Recalling, near wall modelling needs an y^+ less or equal to 1.

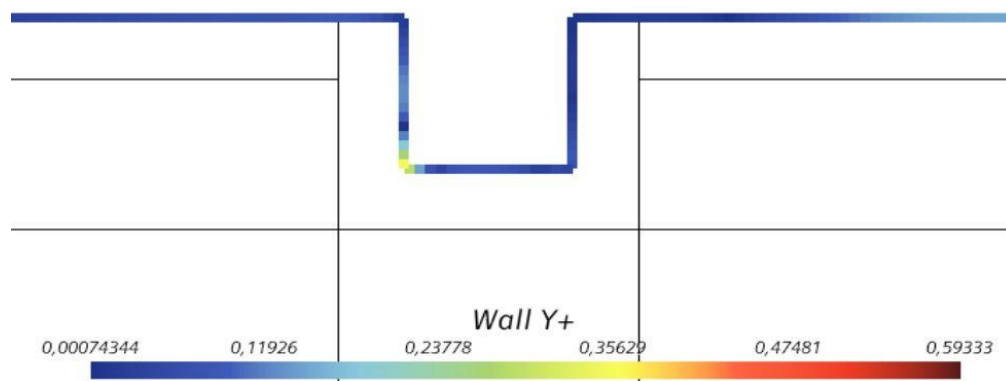


Figure 5.12 - Scalar scene Wall y^+ treatment for rectangular ribs

Briefly are reported the values obtained for each Reynolds number tested in terms of Nusselt and Stanton number, and friction factor:

Tested Reynolds	Nusselt number			Friction factor		
	Experimental procedure	Correlation	CFD analysis	Experimental procedure	Correlation	CFD analysis
20.000	84,74	93,20	164,23	0,018	0,018	0,016
50.000	211,33	212,40	217,62	0,0205	0,0211	0,018
100.000	377,52	388,15	375,106	0,0215	0,0234	0,021

Table 20 - Results in terms of Nusselt number and friction factor with related comparisons for rectangular ribs

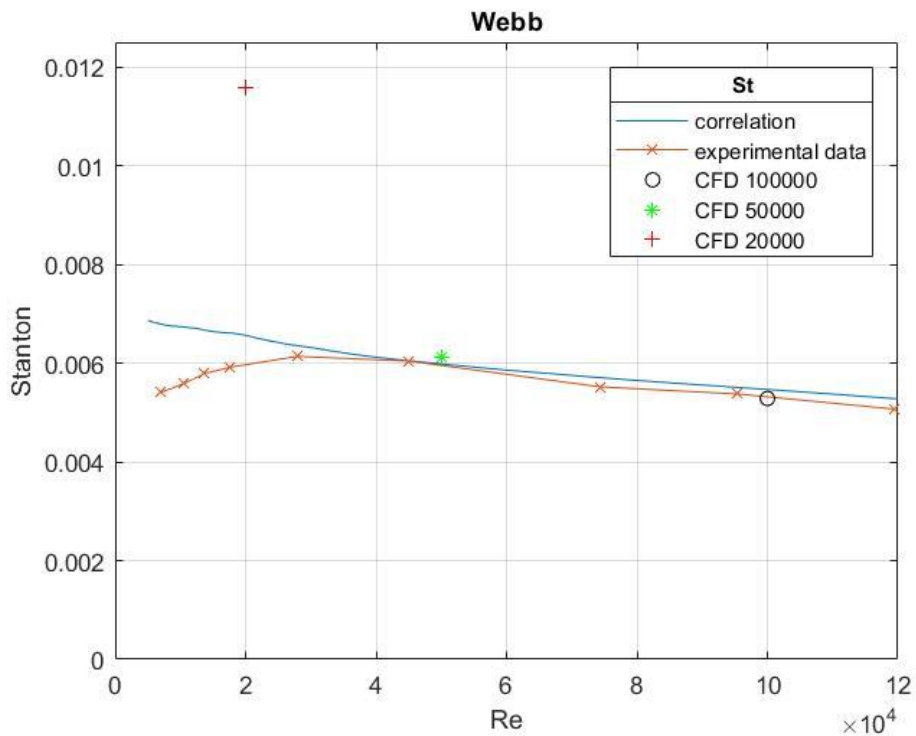


Figure 5.13 - Results in terms of Stanton number (rectangular ribs)

The trend for Nusselt number is coherent to experiments. Figure [5.13] shows that for low Reynolds numbers, the effect of boundary conditions are stronger. The validity of results should be considered reliable in a certain range, firstly because the problem is reduced and then simulations were not performed exactly equal to the experimental procedure and even because boundary such as the flux imposed at the wall was not made explicit by the authors.

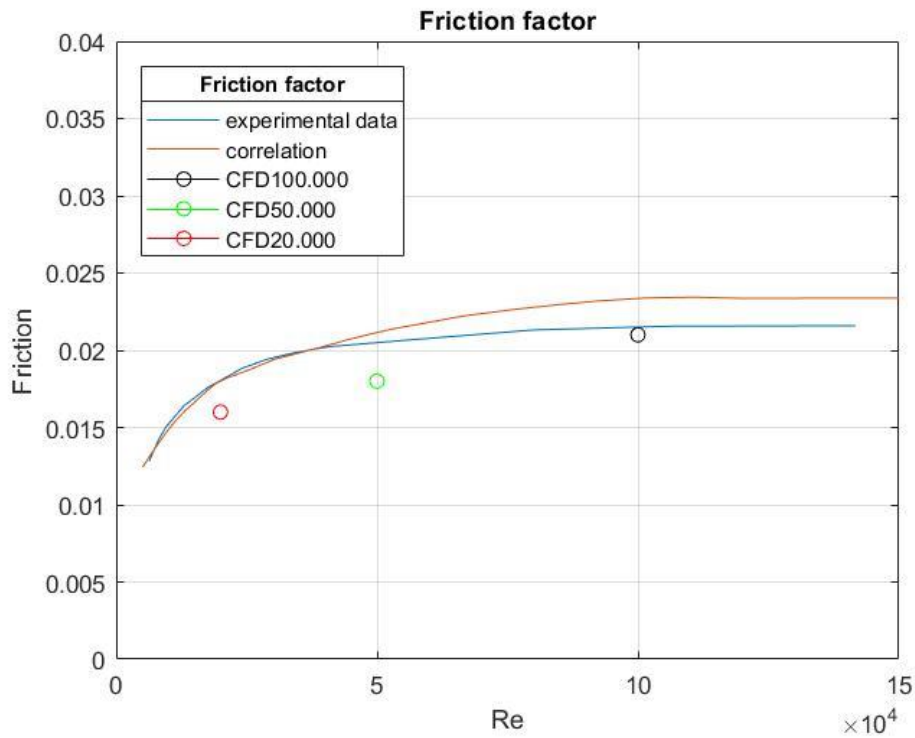


Figure 5.14 - Results in terms of friction factor (rectangular ribs)

For what regards the friction factor, results for different values of Reynolds number do follow the same trend as the experimental ones (and then of correlation indeed).

5.5 Results discussion – Semicircular ribs configuration

In this section results will be showed in the same order as before, starting from the Nusselt number to the Wall y^+ parameter. The results discussed here are taken from the simulation with a Reynolds number equal to 12.000.

Nusselt Number

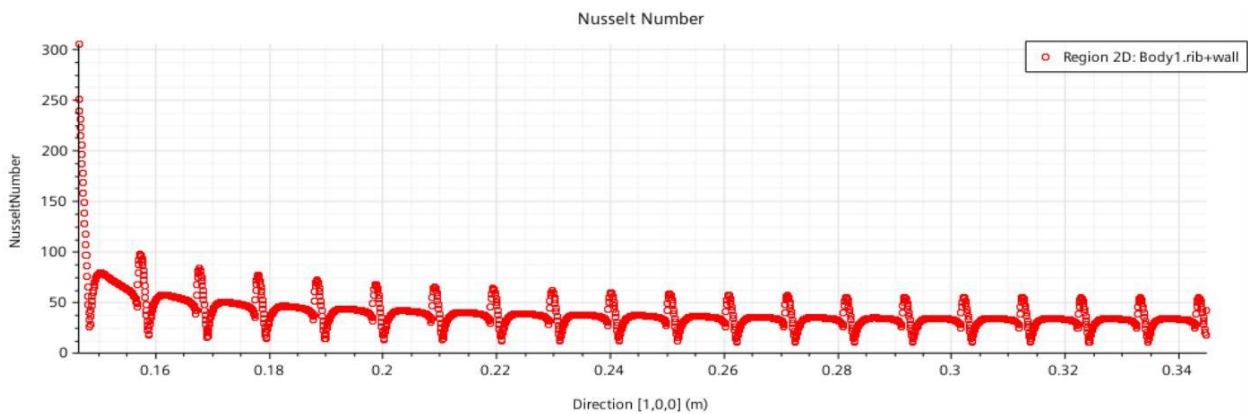


Figure 5.15 - Nusselt number plot from StarCCM+ for semicircular ribs

Again, the average Nusselt number is computed by performing a Surface average evaluation from the Report section. Differently from the rectangular ribs case the fully developed condition from this Plot is reached from the third rib.

Scalar and Vector scenes: Velocity

For what regards velocity, from the scalar scene is clear that the boundary condition is respected, with a mean value of 12,86 m/s.



Figure 5.16 - Scalar scene velocity profile for semicircular ribs

In this case, the vortex formation expected is totally different with respect to the previous case. First of all because of the rib geometry, with a semicircular rib there is not effectively a separation when the flow impacts, but even because the ribs for this case are larger and they do not imply strong effect on the fluid flow in the mean direction.

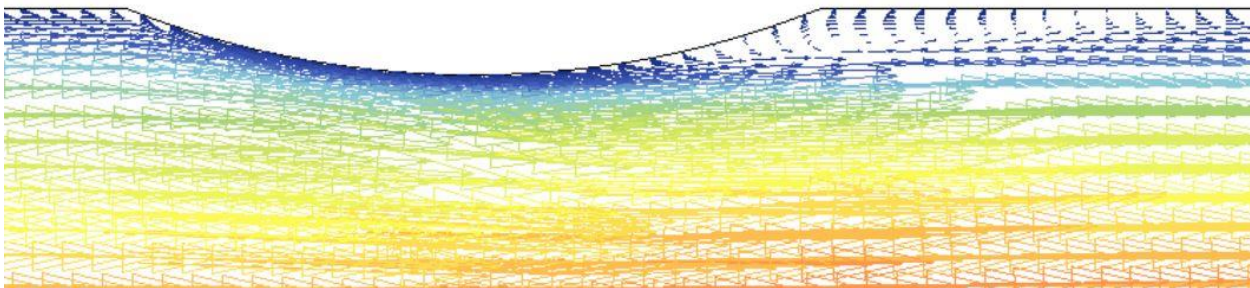


Figure 5.17 - Vector scene velocity profile for semicircular ribs

As anticipated, from the Figure [5.17] a small vortex is generated when the flow overcome the rib. By comparing the Vector scenes of the two cases it can be seen that the size of the vortexes are substantial. Here, the problem of reattachment disappears due to a combined effect of a merely presence of separation and an high value of the rib pitch.

Pressure drop and friction factor

For this case, experiments did not used Adiabatic walls for the evaluation of pressure drops and friction factor. Thus, there was not the need to simulate again the model, but just read the Absolute

Total Pressure values. Again, the choosing of the section was related to the Nusselt number plot, by considering the flow as fully developed from the third rib on.

The same formula as before was taken as reference for the evaluation of the friction factor.

Wall y+

Even in this case the wall y+ is respected because at least it reaches the value of 1.

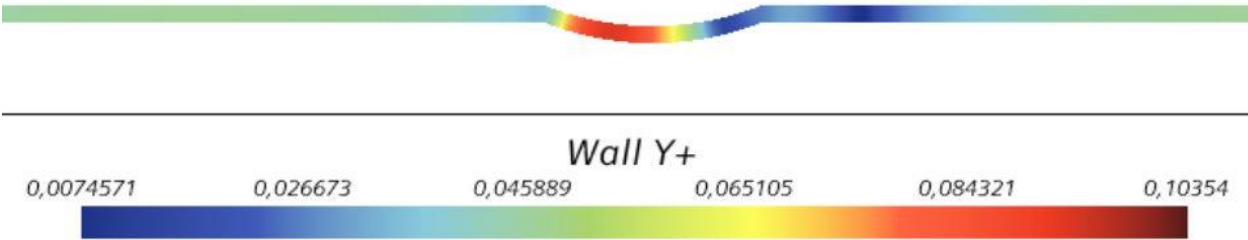


Figure 5.18 - Scalar scene Wall y+ treatment for semicircular ribs

Again, are summarised the values obtained:

Tested Reynolds	Nusselt number			Friction factor		
	Experimental procedure	Correlation	CFD analysis	Experimental procedure	Correlation	CFD analysis
6.000	17,4	17,21	20,78	0,0579	0,0607	0,0482
8.000	23,41	23,27	24,14	0,0557	0,0607	0,0465
12.000	36,43	35,63	37,87	0,0491	0,0512	0,0426

Table 21 - Results in terms of Nusselt number and friction factor with related comparisons for semicircular ribs

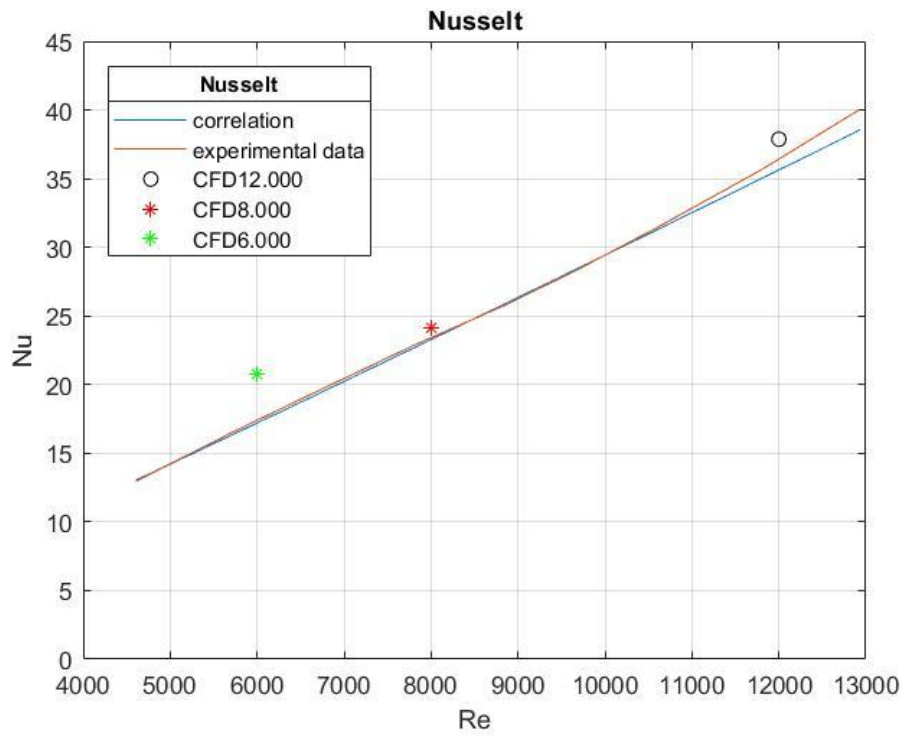


Figure 5.19 - Results in terms of Nusselt number (semicircular ribs)

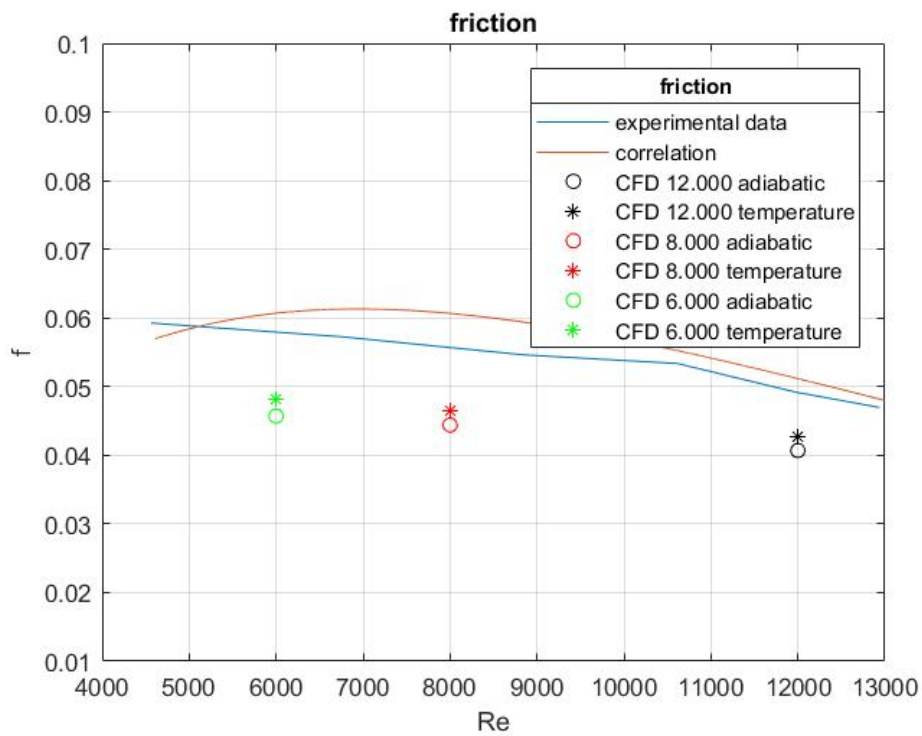


Figure 5.20 - Results in terms of friction factor (semicircular ribs)

Values already listed in the table are now plotted to have a view on the trend which they follow. A comparison between the plot in Figure [5.19] and Figure [5.13] can be done: at low Reynolds number for rectangular case the actual behaviour is slightly different with respect to experimental results, instead in the semicircular case it is almost the same.

Regarding friction factor, the actual values derived from experiments are not catch by the CFD analysis but generally the trend looks really coherent to what predicted.

Chapter 6

6. Final comparison

In this Chapter will be shown how different rib configuration already tested, such as rectangular and semicircular, behave when tested with the same geometry parameters. Thus, as reference were taken values coming from the Matlab plots when pursuing to optimal cases. Recalling, was important to keep the rib pitch-to-height and rib height-to-diameter ratios equal to the optimal ones obtained from correlations:

- $\frac{e}{D} = 0,01$
- $\frac{p}{e} = 10$

For this, the rectangular case resulted to be already tested, while a new geometry for the semicircular rib configuration has been generated. Summing up, geometric parameters for both cases used were:

	Rectangular ribs	Semicircular ribs
Ribbed length [m]	0,07366	0,07366
Entrance length (smooth) [m]	0,3683	0,3683
Exit length [m]	0,3683	0,3683
N° of ribs [/]	20	20
Diameter [mm]	36,83	36,83
Rib height [mm]	0,3683	0,3683
Rib pitch [mm]	3,683	3,683
Rib width [mm]	0,38	0,7366

Table 22 - Geometric values

The two geometries are basically equal, the only difference holds for the rib width which for the semicircular is a bit higher.

Tests were conducted on investigating how the two geometry behave for the same value of the Reynolds number. Therefore, the Reynolds number for this further comparison chosen were:

Reynolds number	12.000	20.000	50.000
-----------------	--------	--------	--------

Table 23 - Tested Reynolds number

It is worth to say that for the semicircular rib configuration this investigation is led ahead of what has been done with experiments by San et al. As a matter of fact, they kept the Reynolds number to a peak equal to 12.936 while now the maximum is 50.000.

The geometry has been imposed always as a 2D domain, holding the same characteristics as before. The only change occurs in the boundary conditions where a different velocity inlet is fixed due to Reynolds number variation.

6.1 New mesh

Surface division

It has been applied a different surface division as:

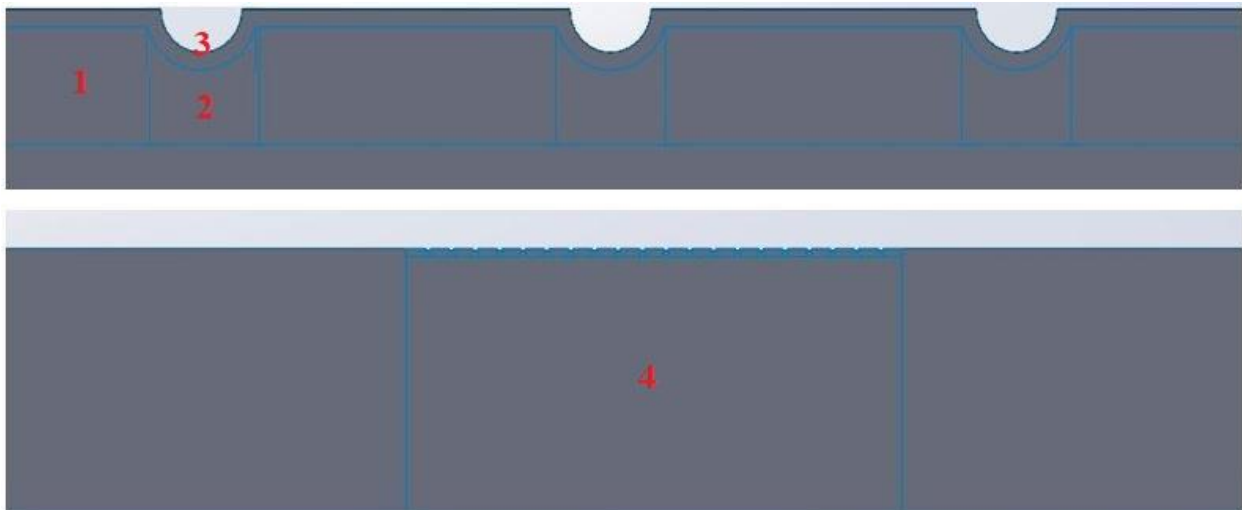


Figure 6.1 - Surface division

For the rectangular case the mesh tested was the same as before (see Figure [5.6]), while for the other a new mesh has been generated due to a change in geometry, ending up with a structured well defined mesh, probably better than what seen before (from Figure [5.7]):

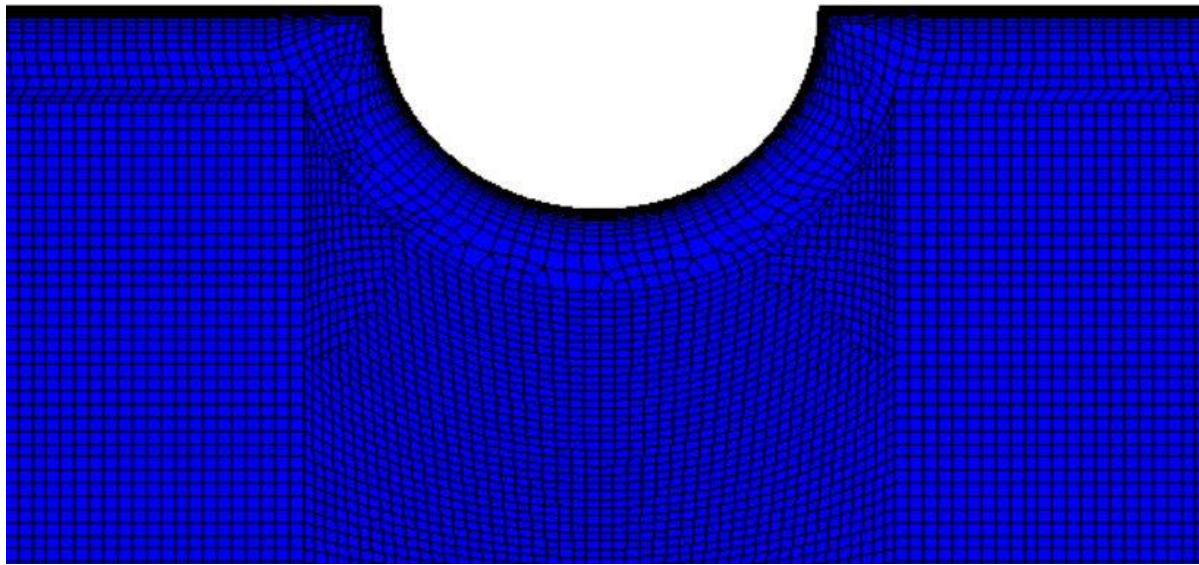


Figure 6.2 - Mesh for the semicircular rib configuration

The only difference here is that the definition of internal surface division is clearer, while for the previous case seemed to show an higher uniformity.

6.1.2 Physics and Boundary conditions

Even the physics is the same as before with the related chosen solvers, explained in Section [5.3.1].

Having said that, are reported the boundary holding for each Reynolds tested:

		Reynolds Number		
Part Surface	Boundary condition	12.000	20.000	50.000
Inlet	Velocity Inlet [m/s]	4,81	8,03	20,08
Outlet	Pressure Outlet [Pa]	0	0	0
Ribbed wall	Wall: Heat Flux [W/m ²]	2500	2500	2500
Entrance+exit walls	Wall: Adiabatic	/	/	/
Side surface	Symmetry Plane	/	/	/

Table 24 - Boundary conditions applied for both cases

6.2 Results in terms of Nusselt number

Here the aspect to be evaluated was mostly regarding the heat transfer capacity of a ribbed channel with whatever configuration. For this, a Nusselt number inspection is done in this section.

In the following plots are depicted the Nusselt number trends with a Reynolds number equal to 50.000.

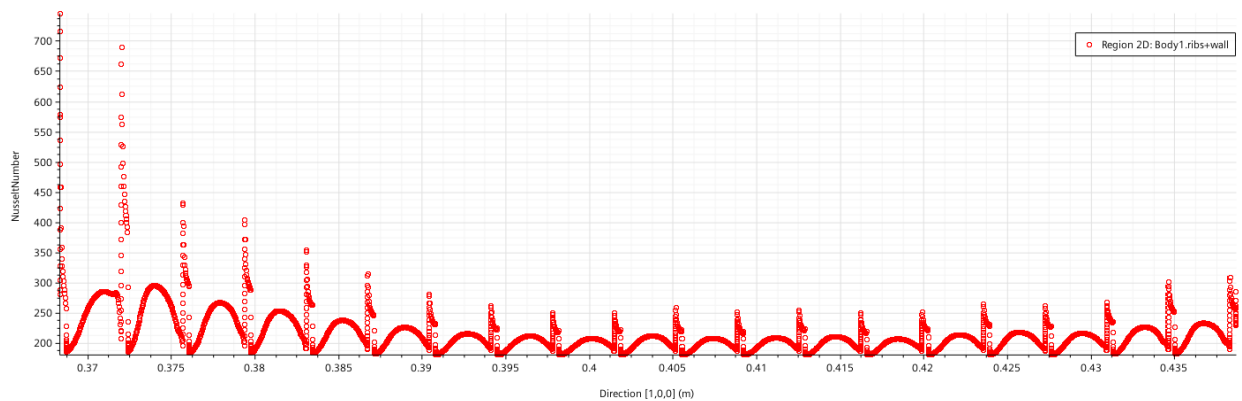


Figure 6.3 - Nusselt number trend for rectangular ribs

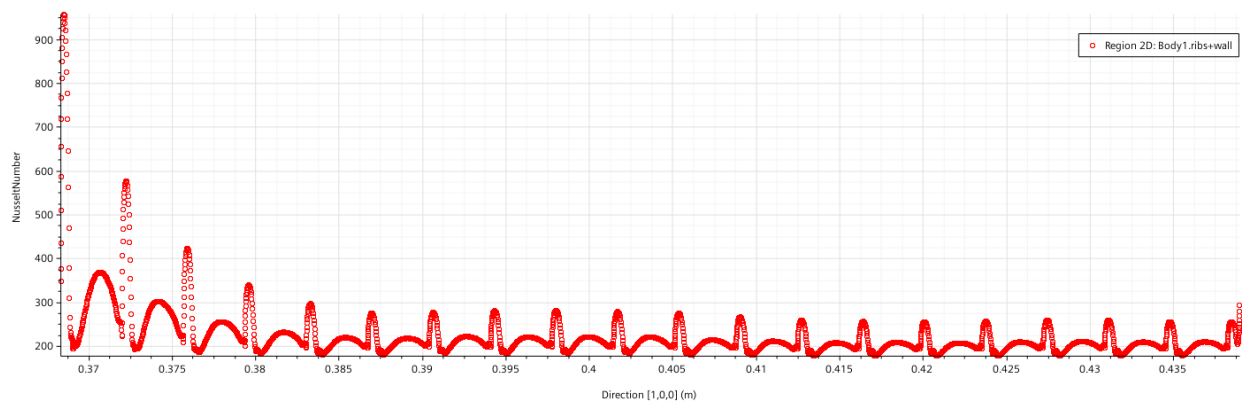


Figure 6.4 - Nusselt number trend for semicircular ribs

From Figure [6.3], slower reattachment of the fluid with the wall while detachment in the rib is evidenced. A higher peak value of the Nusselt is present. For what regards the semicircular ribs configuration (Figure [6.4]):

- faster reattachment of the fluid with the wall
- no detachment from the rib top
- lower peak value

Average Nusselt number values are here reported for each Reynolds number:

<i>Reynolds number</i>	Rectangular ribs	Semicircular ribs
12.000	158,53	156,72
20.000	164,23	170,56
50.000	217,62	224,70

Table 25 - Nusselt number evaluated at each Reynolds

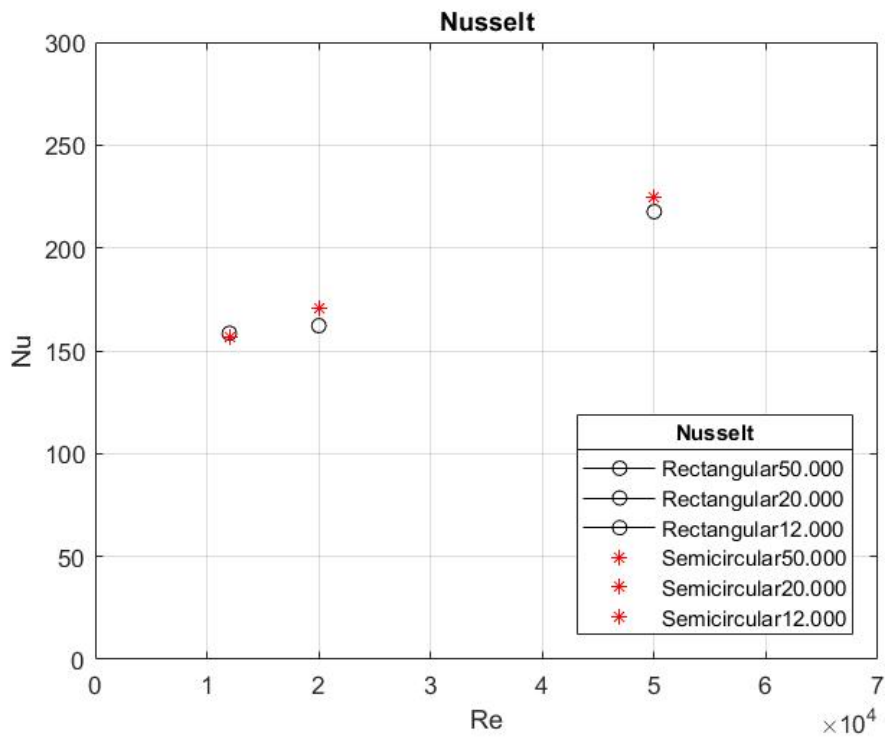


Figure 6.5 - Direct comparison between the two configurations

The trend results to be shared by both cases, with the given boundary conditions. It is evidenced a remarkable increase for semicircular geometry for higher Nusselt number. This point could be enhanced by doing further analyses with higher Reynolds number.

7 Conclusions

7.1 Summarizing conclusions

Objects of the present work are Computational Fluid Dynamic (CFD) analysis of air-cooling flow in a heavy industrial gas turbine blade. These analyses were performed by means of rib-roughened surfaces for internal cooling channels, taking as reference previous studies with the given geometry. The goal was to validate all the models, pursuing to an optimal case just by means of correlations derived experimentally.

First of all, validation was at the very centre of this study. The aim at validating the models was important due to the actual enhancement of convection heat transfer gained with the ribbed surfaces. Then, having found from correlations several configurations which appeared to hold high heat transfer characteristics, a comparison between different rib geometry has been conducted. That was important to establish for further analyses, which case exploited the heat transfer enhancement at its peak.

7.2 Future studies

The present work represents only a home base for future studies. The aim at finding an optimal configuration among the parameters which characterize the fluid flow will be fundamental for gas turbine developments. As introduced, an increase in heat transfer within those channels can be crucial to allow a correct functioning of the whole gas turbine system, avoiding failures due to high thermal gradients and then stresses.

The following analysis which is needed is an evaluation of the optimal configuration reached by means of only CFD study. The correlation analysis was performed to give an understanding of what could happen by implementing that geometry. Of course, general correlation for the ribbed channels used for this study can not be considered as untouchable, so further analyses could result in finding more convenient cases for other rib parameters.

Later, having found the aforesaid parameters, CFD analyses should simulate how they behave when implemented on cooling channels of a turbine blade.

References

- 1- <https://www.ee.co.za/article/development-high-efficiency-flexible-gas-turbine.html>
- 2- Michael E. Lyall, *Heat Transfer from low aspect ratio pin fins*, 2006
- 3- Jenny Sundberg, *Heat Transfer Correlations for Gas Turbine Cooling*
- 4- R.L. Webb, E.R.G. Eckert and R.J. Goldstein, *Heat Transfer and Friction in Tubes with repeated rib-roughness*, 1970
- 5- Jung-Yang San and Wen-Chieh Huang, *Heat transfer enhancement of transverse ribs in circular tubes with consideration of entrance effect*, 2006
- 6- R.L Webb and D.L. Gee, *Forced Convection Heat Transfer in Helically rib-roughened tubes*, 1980
- 7- J.C. Han, L.R. Glicksman and W.M. Rohsenow, *An investigation of Heat Transfer and Friction for rib-roughened surfaces*, 1978